

TP 13244E

**FRACTURE PERFORMANCE
OF NGV CYLINDER DESIGNS**

Prepared for

Transportation Development Centre
Safety and Security
Transport Canada

by

Powertech Labs Inc.

March 1998

TP 13244E

**FRACTURE PERFORMANCE
OF NGV CYLINDER DESIGNS**

by

C.T.L. Webster
and
G.S. Bhuyan
Powertech Labs Inc.

March 1998

This report reflects the views of the authors and not necessarily those of the Transportation Development Centre.

The results and conclusions presented in this report are the views of the authors based on investigations carried out under contract to Gas Technology Canada who subcontracted the work to Powertech Labs Inc. Neither the authors, Gas Technology Canada or its agents, nor the sponsors of the project assume liability for injury or damage resulting from the application of the results and conclusions stated herein.

The Transportation Development Centre does not endorse products or manufacturers. Trade or manufacturers' names appear in this report only because they are essential to its objectives.



1. Transport Canada Publication No. TP 13244E		2. Project No. 8923		3. Recipient's Catalogue No.	
4. Title and Subtitle Fracture Performance of NGV Cylinder Designs				5. Publication Date March 1998	
				6. Performing Organization Document No.	
7. Author(s) C.T.L. Webster and G.S. Bhuyan				8. Transport Canada File No. ZCD1465-650	
9. Performing Organization Name and Address Powertech Labs Inc. 12388-88th Avenue Surrey, B.C. V3W 7R7				10. PWGSC File No. XSD-5-01893	
				11. PWGSC or Transport Canada Contract No. T8200-5-5556	
12. Sponsoring Agency Name and Address Transportation Development Centre (TDC) 800 René Lévesque Blvd. West 6th Floor Montreal, Quebec H3B 1X9				13. Type of Publication and Period Covered Final	
				14. Project Officer Roy S. Nishizaki	
15. Supplementary Notes (Funding programs, titles of related publications, etc.) Sponsored by Program of Energy Research and Development (PERD)					
16. Abstract <p>Natural gas vehicle (NGV) fuel cylinders that remain in service beyond their intended design life can develop fatigue cracks as a result of an excessive number of pressure (fill) cycles. NGV cylinder standards require designs to provide "leak-before-burst" (LBB) performance to prevent rupture in the event that a fatigue crack grows through the wall of metal cylinders or liners. However, the standards do not provide design qualification tests either to demonstrate LBB performance, or to determine the maximum allowable defect size for non-destructive inspection that would ensure the minimum required fatigue life of a design.</p> <p>To identify an LBB performance test, hydraulic and pneumatic burst tests were conducted on various NGV cylinder designs containing flaws machined into the external wall surfaces. It was determined that the hydraulic burst of a cylinder containing a machined flaw could be used to predict whether a flawed cylinder would rupture or leak in compressed gas service. It was concluded that only all-metal (Type 1) cylinders and hoop-wrapped (Type 2) cylinder designs that experience fatigue cracking in the circumferential direction were required to demonstrate LBB performance.</p> <p>Pressure cycling tests were also conducted on Type 1 designs containing various defects machined into the internal and external cylinder walls, to identify a procedure for defining the maximum allowable defect size. It was determined that the most severe test condition involved machining shallow axial defects into the internal surface of cylinders.</p>					
17. Key Words Natural gas vehicle (NGV) fuel cylinders, fracture performance, leak-before-burst, defect size			18. Distribution Statement Limited number of copies available from the Transportation Development Centre		
19. Security Classification (of this publication) Unclassified		20. Security Classification (of this page) Unclassified		21. Declassification (date) —	22. No. of Pages x, 22, apps
					23. Price —



1. N° de la publication de Transports Canada TP 13244E		2. N° de l'étude 8923		3. N° de catalogue du destinataire	
4. Titre et sous-titre Fracture Performance of NGV Cylinder Designs				5. Date de la publication Mars 1998	
				6. N° de document de l'organisme exécutant	
7. Auteur(s) C.T.L. Webster et G.S. Bhuyan				8. N° de dossier - Transports Canada ZCD1465-650	
9. Nom et adresse de l'organisme exécutant Powertech Labs Inc. 12388-88th Avenue Surrey, B.C. V3W 7R7				10. N° de dossier - TPSGC XSD-5-01893	
				11. N° de contrat - TPSGC ou Transports Canada T8200-5-5556	
12. Nom et adresse de l'organisme parrain Centre de développement des transports (CDT) 800, boul. René-Lévesque Ouest 6^e étage Montréal (Québec) H3B 1X9				13. Genre de publication et période visée Final	
				14. Agent de projet Roy S. Nishizaki	
15. Remarques additionnelles (programmes de financement, titres de publications connexes, etc.) Coparrainés par le Programme de recherche et développement énergétiques (PRDE)					
16. Résumé <p>Le fait de maintenir en service au delà de leur durée de vie prévue les bouteilles de gaz naturel pour véhicules risque d'engendrer dans celles-ci des fissures par fatigue résultant d'un nombre excessif de cycles de variation de pression (remplissages). Les normes en vigueur exigent que ces bouteilles respectent un critère de «défaillance non catastrophique», en vertu duquel la propagation d'une fissure par fatigue dans toute l'épaisseur de la bouteille ou de la membrane métallique ne provoquerait pas d'éclatement, mais tout au plus une fuite de gaz. Ces normes ne prévoient pas, cependant, d'essais de qualification destinés à établir la conformité d'une bouteille au critère de défaillance non catastrophique ou de déterminer, aux fins du contrôle non destructif, la dimension maximale de l'amorce de fissure correspondant à la durée de vie en fatigue minimale prescrite.</p> <p>Pour mettre au point un essai de conformité au critère de défaillance non catastrophique, des essais hydrauliques et pneumatiques d'éclatement ont été réalisés sur divers modèles de bouteilles pour véhicules au gaz naturel (VGN) dont la face extérieure présentait des défauts obtenus artificiellement. Les résultats d'essais d'éclatement par mise en pression hydraulique d'une bouteille présentant un défaut intentionnel se sont révélés utiles pour prédire si une bouteille défectueuse de même type éclaterait ou fuirait lorsque chargée de gaz comprimé. Aussi, il s'est avéré qu'il suffisait de soumettre à des essais des bouteilles tout métal (type 1) et des bouteilles frettées par enroulement de fils (type 2) présentant des fissures par fatigue circulaires pour démontrer la conformité de ces bouteilles au critère de défaillance non catastrophique.</p> <p>Des essais de cycles de variation de pression ont également été effectués sur des bouteilles de type 1 affaiblies par des défauts internes ou externes obtenus artificiellement, afin de mettre au point une méthode pour déterminer la dimension maximale admissible d'un défaut. Ces travaux ont révélé que la condition d'essai la plus inclémentaire était celle où des fissures longitudinales de faible profondeur avaient été obtenues artificiellement dans la face intérieure de la bouteille.</p>					
17. Mots clés Bouteilles de gaz naturel pour véhicules, résistance à la rupture, défaillance non catastrophique, dimension d'un défaut			18. Diffusion Le Centre de développement des transports dispose d'un nombre limité d'exemplaires.		
19. Classification de sécurité (de cette publication) Non classifiée		20. Classification de sécurité (de cette page) Non classifiée		21. Déclassification (date) —	22. Nombre de pages x, 22, ann.
					23. Prix —

SUMMARY

Natural gas vehicle (NGV) cylinders are designed for a fixed service life, requiring only periodic visual inspection. A key feature of this limited lifespan is providing a minimum fatigue life. In all-metal (Type1) and metal-lined (Types 2 and 3) designs, an excessive number of pressure cycles will eventually cause fatigue cracks to grow in the metal wall, causing the cylinder to either leak or rupture. To ensure cylinders provide the minimum pressure cycle (fatigue) life, metal cylinders and metal cylinder liners are non-destructively inspected during manufacture to ensure that there are no pre-existing defects present that could cause the premature growth of fatigue cracks. In the event that NGV cylinders inadvertently remain in service beyond their intended lifespan, the cylinder standards require that the failure mode of designs that suffer the through-wall growth of a fatigue crack is by leakage, and not by rupture. This approach is termed “leak-before-burst” (LBB) performance. To comply with the performance basis of the NGV cylinder standards, there is a need to develop test methods that will demonstrate the LBB performance of designs and determine the defect size for nondestructive inspection.

In this study the fracture performance of Type 1 (all-steel and all-aluminum), Type 2 (steel hoop-wrapped and aluminum hoop-wrapped), and Type 3 (aluminum fully-wrapped) NGV designs at 125% of service pressure was investigated by hydraulic and pneumatic burst tests on cylinders into which external flaws had been machined. Pressure cycling tests were also conducted on cylinders containing internal and externally machined defects.

Numerical fracture analysis shows that the crack driving force is greater on the internal surface of a cylinder. Therefore the wall thickness (ligament) remaining under a deep axial crack cut into the external cylinder surface is under a higher crack driving force than the remaining ligament of a deep axial crack cut into the internal cylinder surface. As a result, a burst test of a cylinder containing a deep machined flaw on the external surface in the axial direction would be a conservative test on an all-metal (Type 1) cylinder design to determine whether the design provides LBB performance.

For all-metal (Type 1) cylinders containing machined flaws, it was found that the medium of pressurization (hydraulic or pneumatic) has a significant effect on the failure behaviour of designs which have a low tearing (fracture) resistance. For a machined flaw in a cylinder hydraulically pressurized to failure, an extension of the flaw beyond the machined length was an indication that a rupture could occur under pneumatic conditions. A parametric formula was also developed from sensitivity analysis to calculate the critical flaw length for all-steel cylinder designs.

For hoop-wrapped (Type 2) designs, fracture tests involved a 2 inch (51 mm) long cut through the composite wrap, simulating the kind of damage that could potentially occur under a mounting bracket. In pneumatic pressurization tests on the flawed cylinders, it was demonstrated that a fatigue crack growing in the liner under the damaged composite wrap could only result in a leak failure at 125% of the service pressure. It was concluded that hoop-wrapped cylinders provide leak-before-burst performance, assuming that no significant degradation of the composite wrap has occurred, and that the fatigue cracks in the liner do not grow in the transverse (hoop) direction.

Since numerical fracture analysis shows that the crack driving force is greater on the internal surface of a cylinder, the crack driving force on an internal shallow defect will be more severe than that on an external shallow defect. Pressure cycling tests on a Type 1 cylinder containing shallow defects machined on the internal and external surfaces confirmed the preferential growth of fatigue cracks from the internal defects. As a result, a pressure cycling test of an all-metal or metal-lined cylinder to ensure the minimum fatigue life would require machining a shallow axial defect on the internal surface.

SOMMAIRE

Les bouteilles de gaz naturel pour véhicules sont conçues en fonction d'une durée de vie en service nominale, pendant laquelle elles sont soumises à des inspections visuelles périodiques. En corollaire à cette durée de vie limitée s'impose la nécessité de prévoir une durée de vie en fatigue minimale. Dans les bouteilles tout métal (type 1) et à membrane métallique (types 2 et 3), un nombre excessif de cycles de variation de pression engendre tôt ou tard des fissures par fatigue qui se propagent dans la paroi métallique, entraînant l'éclatement de la bouteille ou une fuite de gaz. Les contrôles non destructifs à l'étape de la fabrication visent à garantir que les bouteilles offrent la durée de vie en fatigue minimale (ou le nombre minimal de cycles de variation de pression). Sont alors rejetées les bouteilles présentant des défauts susceptibles de causer la propagation prématurée de fissures par fatigue. Dans l'éventualité où, par inadvertance, une bouteille serait laissée en service plus longtemps que sa durée de vie prévue, les normes régissant ces appareils exigent que la propagation d'une fissure par fatigue dans toute l'épaisseur de la paroi provoque une fuite de gaz plutôt que l'éclatement. On désigne «défaillance non catastrophique» ce mode de défaillance. Comme toute norme axée sur les performances, les normes relatives aux bouteilles pour véhicules au gaz naturel (VGN) supposent la mise au point de méthodes d'essai permettant de vérifier la conformité des bouteilles au critère de défaillance non catastrophique et de déterminer, aux fins du contrôle non destructif, la dimension maximale de l'amorce de fissure correspondant à la durée de vie en fatigue minimale prescrite.

Au cours de la présente étude, on a examiné la résistance à la rupture de bouteilles pour VGN de type 1 (tout acier et tout aluminium), de type 2 (en acier fretté par enroulement de fils et en aluminium fretté par enroulement de fils) et de type 3 (en aluminium à corps et fonds frettés). Des essais hydrauliques et pneumatiques d'éclatement ont été effectués sur des bouteilles affaiblies par des fissures intentionnelles sur leur face extérieure, chargées à 125 % de leur pression de service. Des épreuves de cycles de variation de pression ont également été réalisées avec des bouteilles présentant des défauts artificiels sur leur face extérieure ou intérieure.

L'analyse numérique du processus de rupture révèle que la force d'extension de la fissure est plus grande sur la face intérieure d'une bouteille que sur sa face extérieure. Ainsi, l'épaisseur de paroi (ou ligament) qui subsiste au fond d'une fissure longitudinale de grande profondeur est soumise à une force d'extension de la fissure plus grande lorsque l'entaille se trouve sur la face extérieure plutôt qu'intérieure de la paroi. On peut donc considérer qu'un essai d'éclatement portant sur une bouteille dont la face extérieure présente une fissure longitudinale intentionnelle profonde permet de se prononcer, avec une marge de sécurité suffisante, sur la conformité d'une bouteille tout métal (type 1) au critère de défaillance non catastrophique.

Dans le cas des bouteilles tout métal (type 1) affaiblies par des défauts intentionnels, il s'est avéré que le fluide utilisé pour la mise en pression (liquide ou gaz) influe grandement sur le mode de défaillance des bouteilles ayant une faible résistance à la rupture. Pour une bouteille affaiblie par une fissure intentionnelle et chargée hydrauliquement jusqu'à la rupture, l'extension de la fissure au delà de la longueur obtenue artificiellement était l'indication d'un risque d'éclatement de la même bouteille chargée pneumatiquement. Une formule paramétrique a également été élaborée à partir de l'analyse de sensibilité, pour calculer la longueur critique de la fissure pour les bouteilles tout acier.

Dans le cas des bouteilles frettées par enroulement de fils (type 2), les essais de rupture mettaient en jeu une entaille de 2 po (51 mm) de longueur dans les frettes en composite, simulant le genre de dommage susceptible de se produire sous un support de montage. Les essais de mise en pression pneumatique réalisés sur des bouteilles défectueuses ont révélé qu'à une pression atteignant 125 % de la pression de service, la propagation d'une fissure par fatigue dans la membrane située sous les frettes entaillées, ne pouvait conduire qu'à une fuite. On peut donc conclure que les bouteilles frettées par enroulement de fils satisfont au critère de défaillance non catastrophique, pour autant que les frettes en composite n'aient pas subi de dégradation importante et que les fissures par fatigue dans la membrane ne se propagent pas circulairement (parallèlement aux frettes).

Comme l'analyse numérique du processus de rupture révèle que la force d'extension de la fissure est supérieure à l'intérieur de la bouteille, il s'ensuit que la force d'extension d'une fissure intérieure de faible profondeur sera plus grande que celle d'une fissure extérieure semblable. Les essais de cycles de variation de pression effectués sur une bouteille de type 1 présentant des fissures intérieures et extérieures intentionnelles peu profondes ont confirmé une tendance plus grande à la propagation des fissures de fatigue intérieures. Donc, pour être valable, un essai de cycles de variation de pression destiné à vérifier la durée de vie en fatigue minimale d'une bouteille tout métal ou à membrane métallique devrait porter sur une bouteille affaiblie par une fissure longitudinale de faible profondeur provoquée artificiellement dans sa face intérieure.

TABLE OF CONTENTS

	<u>Page</u>	
1	OVERVIEW OF RESULTS	1
	1.1 Introduction	1
	1.2 Fracture Performance Investigations	2
	1.3 NDE Defect Size Investigations	9
2	DISCUSSION	12
	2.1 LBB Performance	12
	2.2 NDE Defect Size	14
3	CONCLUSIONS	15
4	RECOMMENDATIONS FOR NGV CYLINDER STANDARDS	16
	REFERENCES	19
APPENDICES		
	A Fracture Performance Test Program	
	B Development of Parametric Equation for Critical Flaw Size Estimation for All-Steel Designs	
	C Numerical Fracture Analysis	

List of Figures	<u>Page</u>
1 Shape of fatigue crack growing from the internal surface of a cylinder	3
2a Machined external flaw (1oT length) before hydraulic pressurization to failure	5
2b After hydraulic pressurization to failure-length of ductile tearing in cylinder wall beyond length of machined flaw (indicates cylinder would have ruptured if pneumatic pressure used)	5
2c After hydraulic pressurization to failure-length of ductile tearing in cylinder wall less than length of machined flaw (indicates cylinder would have leaked if pneumatic pressure used)	5
3a Greater crack driving force associated with the failure of a flaw introduced on the external cylinder surface	12
3b Lesser crack driving force associated with the failure of a flaw introduced on the internal cylinder surface	13

List of Tables

1 Applicable Range of the Terms in the Parametric Formula	9
---	---

1 OVERVIEW OF RESULTS

1.1 Introduction

Natural gas vehicle (NGV) cylinders typically experience a larger number of pressure (fill) cycles than cylinders used in industrial compressed gas service. For example, a 200 bar working pressure (3,000 psi service pressure) cylinder design is required to provide 15,000 pressure cycles from 20 bar to 260 bar (300 psi – 3,750 psi) for a 15 to 20 year life in NGV service [1,2,3]. In all-metal (Type 1) and metal-lined (Types 2 and 3) designs, pressure cycles exceeding the service life requirement will eventually cause fatigue cracks to grow in the metal wall. When a fatigue crack grows through the wall thickness of a cylinder or a liner, the crack will cause the cylinder to either leak or rupture. The failure mode that results depends on the length of the fatigue crack, the fracture toughness of the metal, the internal pressure at the time of failure and the cylinder wall thickness.

The fatigue life of NGV cylinders is a critical design consideration, particularly since these cylinders are only intended to provide a limited service life. To ensure that cylinders provide the minimum pressure cycle (fatigue) life, metal cylinders and metal cylinder liners are non-destructively inspected during manufacture to ensure that there are no pre-existing defects present that could cause the premature growth of fatigue cracks, resulting in failure during the design life of the cylinders. NGV cylinder standards [1,2,3] currently require that fracture mechanics methods be used to calculate the maximum defect size that could exist in the cylinder or liner wall and not affect the minimum fatigue life. This maximum allowable defect size thus becomes the basis of the rejection criteria for non-destructive inspection in the factory. However, this calculation approach typically provides a conservative result and is difficult for independent agencies to verify.

Cylinders are nondestructively inspected during production to ensure that there are no defects that could lead to premature failure by fatigue cracking during the design service life. However, NGV cylinders may inadvertently remain in service beyond their intended life span, possibly resulting in eventual failure by fatigue cracking. For NGV cylinder designs that remain in service for up to three times their intended service life, the required failure mode is leakage – not

rupture. This approach is termed “leak-before-burst” (LBB) performance. NGV cylinder standards [1,2,3] currently require that fracture mechanics calculations be used to demonstrate the LBB performance of a design. As with the calculation of the maximum defect size, this method typically provides a conservative result and is difficult for regulatory agencies to verify.

Consistent with the philosophy of a performance standard for NGV cylinders, and to simplify the acceptance of test results, the need exists to define tests that can be used to demonstrate LBB performance of cylinder designs and determine the defect size for non-destructive inspection.

1.2 Fracture Performance Investigations

1.2.1 LBB Background

The objective was to determine whether the failure mode (rupture or leak) of a cylinder containing a fatigue crack under pneumatic conditions could be predicted by the hydraulic burst of a cylinder containing a flaw machined into the external surface. Factors to consider are as follows:

- Whether a flaw machined on the external surface is representative of a fatigue crack growing from the inside surface of a metal cylinder or liner.
- The large difference in the amount of energy released when the cylinder fails between a compressed gas (pneumatic) and an essentially incompressible fluid (hydraulic).
- The length of machined flaw that would be representative of a fatigue crack failure.

Fatigue cracks typically initiate on the inside walls of a cylinder (due to the fact that higher crack driving forces are often present on the inside surfaces of designs) and grow outward in a semi-elliptical shape (see Figure 1). A cylinder containing a fatigue crack would likely fail during a filling operation when the pressure would tend to reach a maximum.

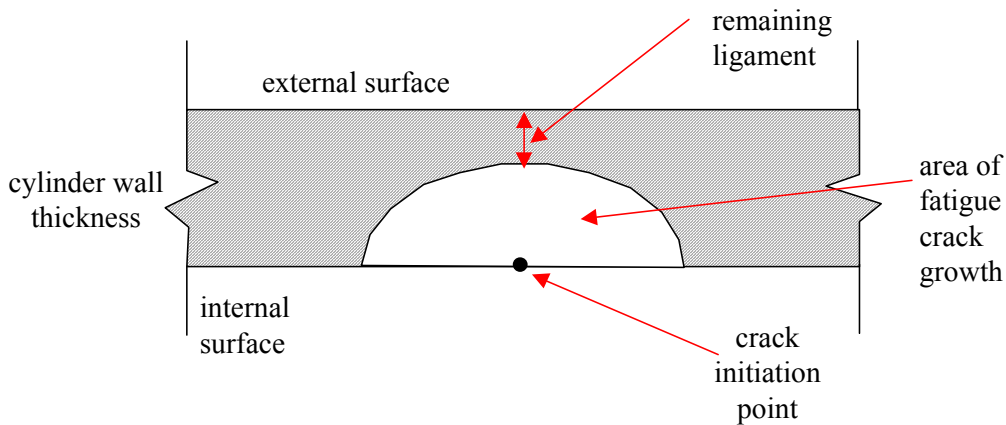


Figure 1: Shape of fatigue crack growing from the internal surface of a cylinder.

A fatigue crack failure could be simulated by cutting a flaw into the wall of a cylinder, then pressurizing the cylinder to cause it to fail. The size of the flaw would be such that the cylinder would fail when it was pressurized to about the maximum fill pressure. However, it was not known whether the simplified approach of cutting a flaw inward from the outside surface would adequately represent the failure mode that would actually occur in service, since fatigue cracks typically grow outward from the inside surface. In addition, introducing flaws into the external surface of the metal liners of hoop-wrapped (Type 2) cylinders would necessarily involve cutting through the composite wrap, making for a more severe test condition in these designs.

The use of a compressed gas to pressurize a flawed cylinder to failure is dangerous since a rupture would involve the release of tremendous force. A hydraulic fluid, such as water, is a more convenient and safer test medium for pressurization to failure, since the relative incompressibility of fluid results in significantly less energy being released during a cylinder failure. However, a correlation between the effect of using a pneumatic and a hydraulic medium on the failure mode of a cylinder has not been demonstrated for NGV cylinders. As a result, pressurizing a flawed cylinder to failure using a fluid medium may result in only a leak, while using a compressed gas may result in a rupture.

1.2.2 LBB Approach

An analysis of the stresses associated with a crack in the wall of a cylinder (see Appendix C) determined that externally machined flaws actually provided a more severe test of LBB performance. This occurs because the crack driving force on the internal surface of a cylinder is higher than that on the external surface; consequently, the remaining ligament of a flaw machined into the external surface of a cylinder will be under a higher force at the moment of failure than the remaining ligament of a fatigue crack growing outward from the internal surface of a cylinder. As a result, all burst tests were conducted using either water or compressed nitrogen on cylinders containing flaws machined into the external surfaces. The resulting cylinder fractures were then compared to determine if any relationship existed.

Concurrent with the burst testing of flawed cylinders, an investigation was conducted by Cyltek, Inc., to establish a calculation method to predict the LBB performance of steel cylinders. A parametric equation was developed and validated using the results of the pneumatic burst tests. The equation is provided in Section 1.2.6.

1.2.3 LBB Performance of Type 1 All-Metal Cylinders

Pneumatic and hydraulic burst tests were conducted on AISI 4130X steel cylinders containing externally machined flaws. The cylinders, manufactured by Faber Industrie and Taylor Wharton, were determined to represent opposite ranges of fracture toughness values for steels used in NGV service. Test details are provided in Appendix A.

Flaws of various lengths and depths that would cause failure to occur during pressurization between the service pressure and the maximum fill pressure (1.25 times the service pressure) were machined into the external surfaces of cylinders. For steel cylinders the results of numerous pressure cycling tests to failure conducted in this study and elsewhere [4,5] determined that the length of fatigue cracks typically vary from 2 to 7.5 times the wall thickness (2T to 7.5T). Most tests involved a 10T flaw length (see Figure 2a), comparable to the flaw size required by the ISO TC 58/SC 3/WG 14 working group for ensuring adequate fracture toughness of high-strength industrial gas cylinders [6].

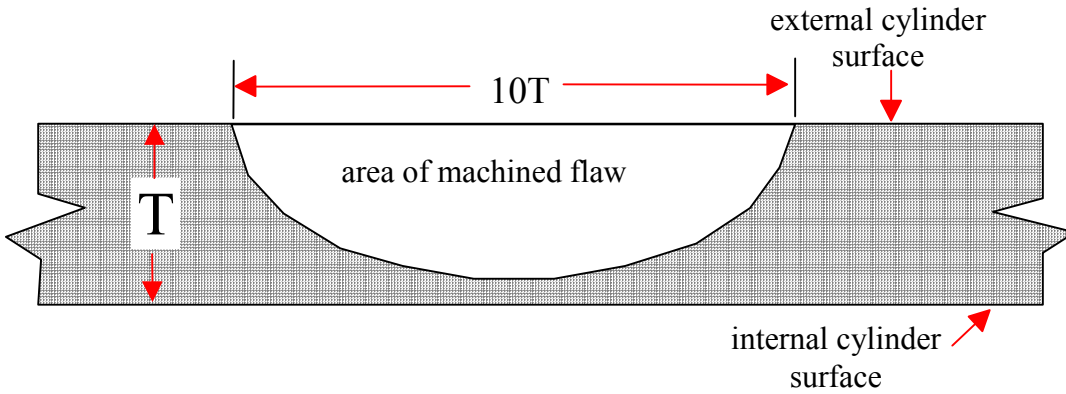


Figure 2a: Machined external flaw ($10T$ length) before hydraulic pressurization to failure.

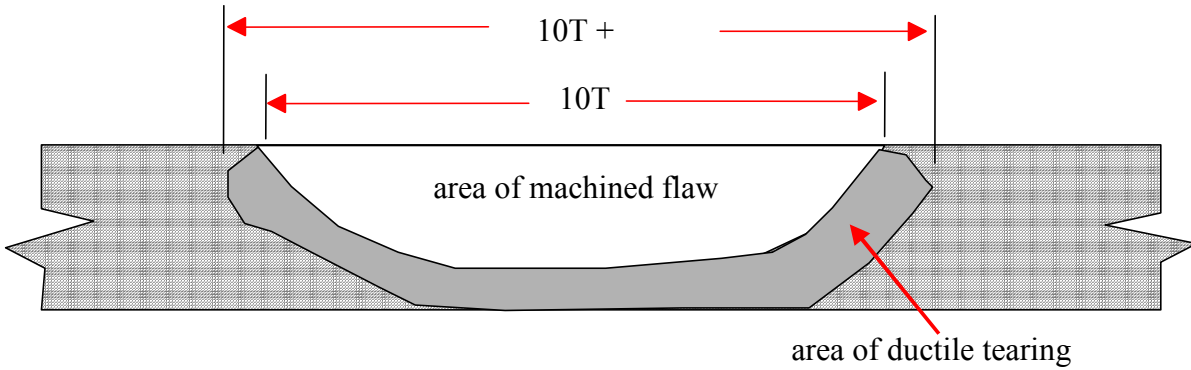


Figure 2b: After hydraulic pressurization to failure – the length of ductile tearing ($10T+$) beyond the machined flaw length ($10T$), indicating the cylinder would have ruptured if pneumatic pressure used.

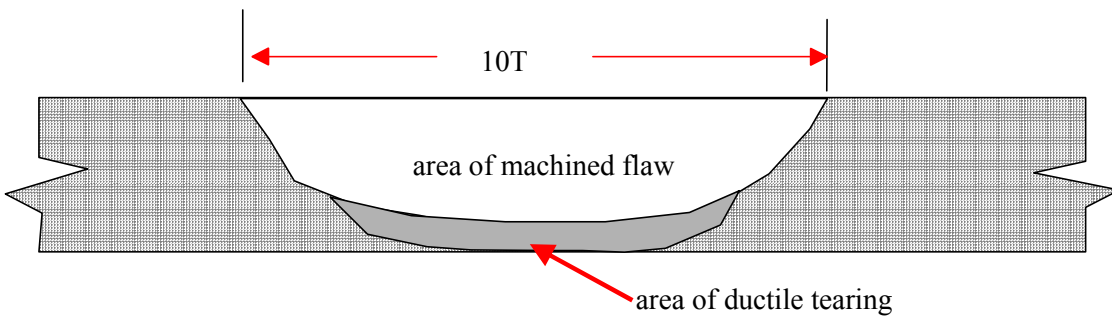


Figure 2c: After hydraulic pressurization to failure – the length of ductile tearing is less than the machined flaw length, indicating the cylinder would have leaked if pneumatic pressure used.

It was found that the Taylor Wharton cylinder design containing a flaw of 10T length and of sufficient depth ruptured when pneumatically pressurized to 1.25 times its service pressure. In comparison, the same design with the same flaw size leaked when it was hydraulically pressurized to about the same pressure. Examining the fracture surface of the leak cylinder, it was found that the hydraulic pressurization had caused extension (ductile tearing) of the metal some 7% beyond the machined length of the flaw (see Figure 2b). This observations indicates that the results of a hydraulic burst test of a flawed cylinder could be used to predict the failure mode if compressed gas had been used instead.

For the Faber cylinder design, cylinders containing flaws of up to 12.5T would leak when pressurized pneumatically to the maximum fill pressure. Faber cylinders containing the same flaw size also leaked when hydraulically pressurized to a similar pressure. In the hydraulic test, there was no evidence of any ductile tearing in the metal beyond the length of the machined flaw (see Figure 2c).

Pneumatic and hydraulic burst tests were also conducted on AA6061-T6 and AA7032 aluminum cylinders, all manufactured by Luxfer USA. The test results are discussed in detail in Appendix A.

Pressure cycling both aluminum cylinder designs to failure provided fatigue crack lengths that were typically 4 to 5 times the wall thickness (4T to 5T). For the AA6061 design the fatigue crack failures were in the circumferential direction due to the flat shape of the cylinder end. Since a circumferential flaw is difficult to machine into the external surface of a cylinder, all flaws used in this test program were machined in the longitudinal (axial) direction.

For the AA6061 design, it was found that the cylinder would rupture when a flaw of 6T length and of sufficient depth was pressurized pneumatically to the maximum fill pressure. Shorter flaw lengths would only result in a leak when pneumatically pressurized to between the service pressure and the maximum fill pressure. For the same size of flaw, the cylinder would leak when pressurized hydraulically to a similar pressure. However, examining the fracture surfaces revealed that the hydraulic failure had caused ductile tearing to occur in the metal extending

some 6% beyond the length of the machined flaw. This indicated that the inspection of fracture faces following a hydraulic burst test of a flawed aluminum cylinder could be used to predict whether a rupture would occur when pneumatic pressure was used.

For the AA7032 design, the results of hydraulic burst tests on flawed cylinders caused the manufacturer to believe that rupture would occur under pneumatic conditions if a crack grew through the sidewall of the cylinder. As a result, during production the manufacturer machined an external “starter” notch into the base of these cylinders. Pressure cycling these notched cylinders to failure demonstrated that fatigue cracking would always initiate at the notch and grow inwards. Pneumatic burst testing of a cylinder containing a flaw of 9.4T length in the cylinder base resulted in only a leak failure.

1.2.4 LBB Performance of Type 2 Hoop-Wrapped Cylinders

Pneumatic and hydraulic burst tests were conducted on hoop-wrapped aluminum (AA6061-T6) cylinders manufactured by CNG Cylinder Company, and on hoop-wrapped steel (AISI 4130x) cylinders manufactured by Pressed Steel Tank. Flaws were introduced into the external surface of the metal liners by cutting completely through the FRP hoop-wrap. These flawed cylinder tests represent an exceptionally severe test condition, since in service it would be expected that a fatigue crack would eventually grow through the liner without the FRP wrap being damaged. Test details are provided in Appendix A.

The cuts through the FRP wrap were 2 inches (51 mm) in length, approximating the extent of mechanical damage that can occur from improperly installed mounting brackets. The cut depths penetrated completely through the wrap and into the liner, to a depth that would cause the cylinders to fail when pressurized to between the service pressure and the maximum fill pressure. In all cases the cylinders leaked when pneumatically pressurized to failure.

To determine whether the bare end domes of hoop-wrapped cylinders provide LBB performance, a flaw was externally cut into the dome of an aluminum hoop-wrapped cylinder. The aluminum hoop-wrapped design was selected for this test since aluminum alloys have less fracture toughness than steel. When pneumatically pressurized to failure, the cylinder leaked at the dome

flaw. This confirmed the fact that the ends of cylinders should provide LBB performance because of the lower stresses compared to the cylindrical wall of cylinders, and the ends are typically thicker.

1.2.5 LBB Performance of Type 3 Fully-Wrapped Cylinders

The composite wrap of Type 3 cylinders carries the majority of the structural load, thus a fatigue crack growing through the metal liner could only result in a leak. While this type of design is already considered to provide LBB performance, several pneumatic burst tests of flawed cylinders were conducted to demonstrate this performance.

In one test, an external flaw of 3 inches (76 mm) length was cut through the composite wrap and into the metal liner of a fully-wrapped cylinder made by Structural Composites Industries. Since the composite wrap was cut, this type of damage was significantly more severe than a fatigue crack simply growing through the metal liner. When pneumatically pressurized to 2,715 psi (18.7 MPa), the cylinder failed by leaking.

In a test performed under another project, a fully-wrapped cylinder manufactured by Dynetek Industries was filled with compressed hydrogen and pressure cycled to failure. The cylinder failed at 3,750 psi (26.7 MPa) by leaking when a fatigue crack grew through the aluminum liner [7].

1.2.6 LBB Calculation Formula for Type 1 Steel Cylinders

A program called C-LBB (Cylinder LBB) was used by Cyltek to calculate “critical crack” sizes for all-steel cylinders i.e., the crack length at which the failure mode would transfer from leak to burst. Various sensitivity analyses were carried out, taking into account variations in cylinder size, yield strength, stress level and fracture resistance of materials. The analyses used the failure assessment diagram (FAD) based on the R6 level 3 procedures [8]. In the assessments, cracks were modelled as through-wall cracks. The parametric formula shown in Equation 1 was developed by Cyltek to estimate critical crack length for an all-steel cylinder design for LBB

performance. A crack greater than the estimated length “L_d” for a particular design is predicted to exhibit rupture failure mode.

$$L_d = 0.00038 \cdot RT^{0.473} \cdot \sigma_y^{2.087} \cdot \left(\frac{J_1}{1000}\right)^{0.446} \cdot \sigma_H^{0.013J_1} \cdot \exp\left[-0.024\sigma_H - 0.008\sigma_y + 0.1\left(\frac{J_0}{1000}\right) - 0.064\left(\frac{J_1}{1000}\right)\right] \quad (1)$$

where L_d is the estimated crack length in inch, R, is the outer radius in inches, T is the wall thickness in inches, σ_y is yield strength in ksi, σ_H is hoop stress in ksi, J₀ resistance curve intercept in in-lb /in² x 10³ and J₁ resistance curve slope, in in-lb/in x 10³.

The applicable range for the terms in Equation 1 is given in Table 1.

Table 1. Applicable Range of the Terms in the Parametric Formula.

Term	Description	Range
RT	Cylinder size-outside radius x wall thickness (in ²)	0.5 < RT < 5
σ _y	Yield Strength (ksi)	90 < σ _y < 200
σ _H	Hoop Stress (ksi)	50 < σ _H < 100
J ₀	Resistance Curve Intercept (in-lb/in ² x 10 ³)	0.2 < J ₀ < 1.0
J ₁	Resistance Curve Slope (in-lb/in x 10 ³)	0 < J ₁ < 60

The developed parametric formula [Eqn. 1] was compared with the flawed cylinder burst test data generated from this project as well as from the ISO WG 14 program [6]. The comparison was reasonably accurate, and is contained in Appendix B, along with details of the development of the formulae.

1.3 NDE (non-destructive evaluation) Defect Size Investigations

1.3.1 Background

The objective was to define a performance test that could be used to establish the defect size for the non-destructive inspection of cylinders in the factory to ensure a minimum pressure cycle (fatigue) life. The approach adopted in the present study involved introducing a defect of some specified length and depth into the cylinder wall, then pressure cycling the cylinder from 300 psi (2.07 MPa) to 1.25 times the service (working) pressure until failure. If that fatigue failure did

not occur within the 15- or 20-year design life of the cylinder, this initial defect depth would provide the basis for an NDE rejection criterion.

Fatigue cracks typically initiate at defects on the internal surface of cylinders where the crack driving force is greater (see Appendix C). Fatigue cracks also require an incubation period to initiate and grow. Among other factors, the incubation time depends on the “sharpness” (stress concentration) along the tip of the defect. The crack initiation time can also be reduced by the superficial pitting corrosion that sometimes occurs on the internal surfaces of steel cylinders [4]. In-service fatigue cracks may also experience some accelerated growth due to the possible contribution of corrosion mechanisms (corrosion fatigue).

Because of the variability in fatigue crack initiation time and rate of crack growth which may be caused by the factors listed above, a defect size performance test would necessarily be limited to the use of defects that have a depth of 5% or less of the cylinder wall thickness. Non-destructive examination to reject industrial cylinders containing defects greater than 5% of the wall thickness has been in use for a number of years [9]. In addition, steel cylinders that were ultrasonically inspected in the factory to eliminate defects greater than 5% of the wall thickness, had not experienced any significantly greater depth of defects after up to 13 years of NGV service [4]. This finding indicates that for cylinders with initial defects less than 5% of the wall thickness in depth, the crack incubation times and crack growth rates that occur in service do not have any substantial effect on the design life of the cylinders.

1.3.2 Defect Size Approach

To determine the machining method that would create the most rapid initiation of crack growth, various techniques were used to introduce defects of approximately the same length and depth into the external sidewall surfaces of a Faber steel cylinder and a Luxfer AA6061 aluminum cylinder. The cylinders were then pressure cycled to failure from 300 psi (2.07 MPa) to 3,750 psi (25.85 MPa), and the resulting amount of fatigue crack growth from each of the various cuts was determined.

To determine how the location (internal or external) affects the rate of crack initiation and growth, defects of 10T length and of various depths were introduced into both the internal and external surfaces of a Faber steel cylinder using electro-discharge machining (EDM). The cylinder was then pressure cycled to failure from 300 psi (2.07 MPa) to 3,750 psi (25.85 MPa).

1.3.3 Results of NDE Defect Machining Method Tests

In the Faber steel cylinder containing the multiple machined defects, failure occurred in the defect cut by a 30° CVN cutter. The next greatest amount of crack growth occurred in the grinding mark, followed by the EDM and the 45° CVN cutter defects. In the Luxfer AA6061 aluminum cylinder containing the multiple machined defects, failure occurred at the EDM defect. The next greatest amount of crack growth occurred in the 30° CVN cutter defect. Both the EDM and 30° CVN cutter methods provided similar profiles in the base of the defects, characterized by relatively sharp corners. Test details are provided in Appendix A.

For the location test, fatigue crack growth first initiated at the deeper cuts (up to 13% of T) made on the external surface of the Faber steel cylinder; however, the fatigue failure occurred at an internal defect with an initial depth of only 6% of T. This result illustrates the higher crack driving force typically present on the internal surfaces of cylinders. Test details are provided in Appendix A.

2 DISCUSSION

2.1 LBB Performance

Fatigue cracks initiate at some pre-existing defect, such as a score mark from manufacturing, or corrosion from some exceptional cause, on a cylinder surface. The length of the resulting fatigue crack is usually a function of the size of the pre-existing defect. The length of through-wall fatigue cracks typically varies from 2 to 7.5 times the cylinder wall thickness.

During design qualification testing, the pressure cycling of virgin cylinders to failure may not necessarily produce fatigue cracks with representative lengths. To account for variations that occur in manufacturing, it is recommended that the resulting fatigue crack length be multiplied by a factor of 2 prior to using the crack length as the basis for machining a flaw into a cylinder and hydraulically burst testing the cylinder to demonstrate LBB performance.

It was determined from Appendix C that the crack driving force is greater on the internal surface of a cylinder. As a result, an axial crack introduced into the external surface of a cylinder will have a greater crack driving force present on the remaining ligament (see Figure 3a) than the crack driving force that would be present on the remaining ligament of an axial crack introduced

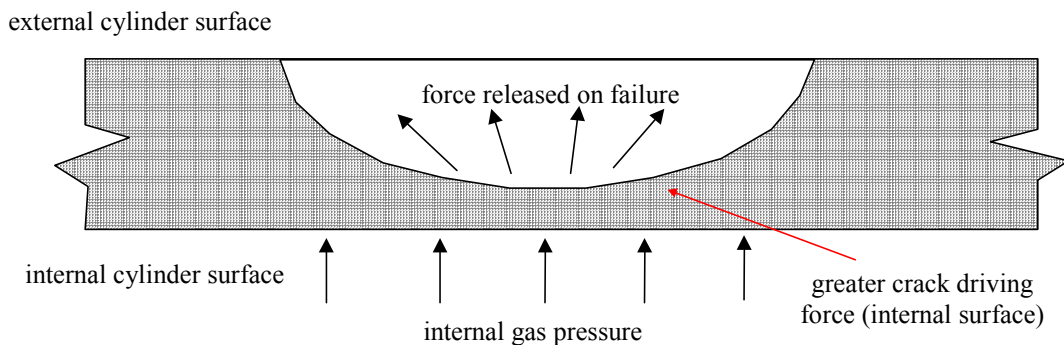


Figure 3a: Greater crack driving force associated with the failure of a flaw introduced on the external cylinder surface.

into the internal surface of a cylinder (see Figure 3b). Thus compared to an internal flaw, a greater force would be associated with the failure of an external flaw in a cylinder. Test results also indicate that if the length of a machined flaw in a cylinder increases during a hydraulic burst at or above the maximum fill pressure, the design would likely experience rupture under pneumatic burst conditions.

In certain cylinder designs, the fatigue crack will not preferentially grow in a location or

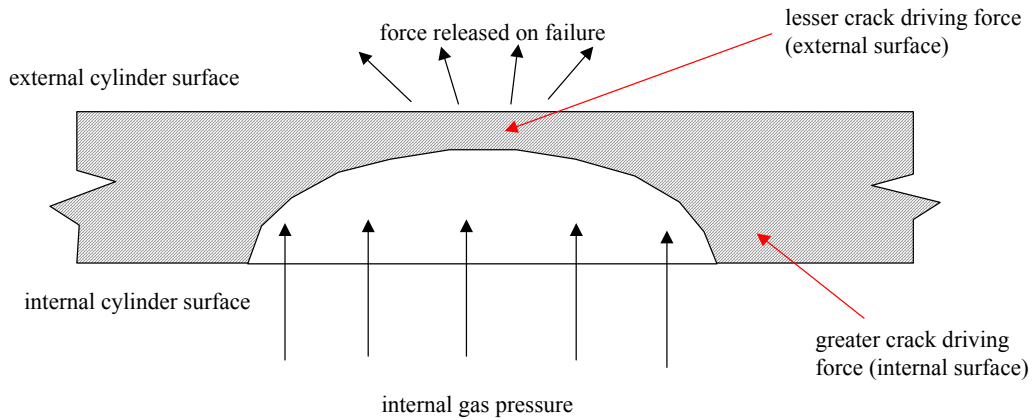


Figure 3b: Lesser crack driving force associated with the failure of a flaw introduced on the internal cylinder surface.

direction conducive to the machining of an external flaw for LBB burst testing. In these designs, a starter notch of controlled dimensions could be used in all production cylinders to fix or control the location and orientation of a fatigue crack. Similarly, in designs where the fatigue crack lengths that result from pressure cycling to failure would prevent the design from providing LBB performance, the use of a starter notch on all production cylinders could be used to control the length of fatigue cracks. The Luxfer AA7032 design provides an excellent example of how a starter notch can be used to control the size and location of a fatigue crack to provide LBB performance, while still permitting the design to provide the necessary minimum fatigue life.

For hoop-wrapped designs, the pneumatic pressurization testing to failure of cylinders containing flaws cut completely through the composite wrap and into the liners demonstrated that composite-wrapped designs inherently provide LBB performance, provided the composite wrap has not been severely damaged in service. The composite wrap functions as a crack arrester to prevent crack propagation. In addition, the lower stresses associated with the geometry and thickness of the unwrapped dome ends of hoop-wrapped cylinders also provide an inherent LBB performance. This was demonstrated by leakage of an aluminum hoop-wrapped cylinder containing a gross flaw cut into the end dome that was pneumatically pressurized to failure.

However, Type 2 (hoop-wrapped) designs that tend to develop fatigue cracks in the circumferential direction, in particular designs with flat-bottoms, may not provide LBB

performance. For such designs, an LBB performance test would be difficult to conduct, thus it would be necessary to prevent fatigue cracking in the circumferential direction.

2.2 NDE Defect Size

The results of both the numerical fracture analysis (Appendix C) and the pressure cycle tests on internal and external cylinder flaws demonstrated that fatigue cracking typically grows more rapidly from the internal surface of a cylinder design. As a result, defects introduced into the walls of cylinders for pressure cycling to define an NDE defect size should be machined on the internal surfaces of Type 1, Type 2 and Type 3 cylinder designs. This machining on the internal surface of the cylinder or liner would probably have to be accomplished prior to spinning (or forming) the end closed. The NDE method used by the manufacturer must be shown capable of detecting the length and depth of the defect.

It would appear that the electro discharge machining (EDM) and the 30° CVN cutter typically provide the least crack incubation times in steel and aluminum cylinder designs. However, there will always be some variability in how machined defects are introduced, thus there will be some variation in the fatigue life obtained from the defects. To account for this irregularity, the maximum allowable depth for these NDE defects should be limited to 5% of the wall thickness. This 5% limit is consistent with the current NDE inspection requirements for transportable gas cylinders.

Sharper edges on a machined defect result in higher stresses and less crack incubation time.

3 CONCLUSIONS

1. The medium of pressurization (i.e. pneumatic or hydraulic) can have a significant effect on the appearance of the failure mode of cylinders. Tested to the same pressure, a flawed cylinder that leaks under hydraulic pressure could rupture under pneumatic pressure.
2. The hydraulic burst of a cylinder containing a flaw machined into the external surface can be used to predict the failure mode (leak or rupture) of a flawed cylinder under pneumatic burst conditions.
3. Composite-wrapped cylinder designs provide leak-before-burst performance in the event that a fatigue crack grows through the metal liner, assuming the surrounding wrap has not degraded significantly.
4. A notch machined into cylinders during production can be used to control the size and location of an eventual fatigue crack.
5. A parametric equation has been developed for Type 1 steel cylinders to estimate the limiting crack size at which a change from a leak mode to a rupture mode of failure would occur.
6. Shapes of machined defects introduced by the EDM technique and by a CVN cutter with a 30° angle are very similar, and have been observed to initiate fatigue cracking in cylinders subjected to cyclic pressurization before defects introduced using other machining techniques.

4 RECOMMENDATIONS FOR NGV CYLINDER STANDARDS

1. Determination of LBB performance is only required for Type 1 (all-metal) cylinder designs, and for Type 2 (hoop-wrap) designs where the fatigue crack typically grows in the transverse (circumferential) direction.
2. For Type 1 (all-metal) cylinder designs LBB performance can be demonstrated by the following test method:
 - a) Pressure cycle three or more cylinders to failure from 300 psi (2.07 MPa) to 1.25 times the service (working) pressure.
 - b) The length of the longest through-wall fatigue crack found on the three cylinders (as measured on the initiation side of the crack) shall be multiplied by 2 and used for the flawed cylinder burst tests.
 - c) The longest crack length (multiplied by 2) shall be machined into the external sidewall surface of at least three cylinders using either electro-discharge machining, or a 30° Charpy V-notch cutter with a diameter of 3-4 inches (76-101 mm), a thickness of 0.0625 inches (1.6 mm) or less, and a tip radius of 0.010 inches (0.25 mm) or less.
 - d) The depth of the machined flaw shall be sufficient to cause a hydraulic burst pressure of at least 1.25 times the service (working) pressure.
 - e) The fracture surfaces of the three cylinders shall be examined to confirm that the fracture did not extend beyond the machined length of the flaw.
3. For Type 1 and Type 2 cylinder designs which do not consistently experience fatigue failure in the axial direction, or cannot provide LBB performance using the fatigue location or crack size determined from the pressure cycling of three cylinders to failure, a machined notch may be used to control the location and size of a fatigue crack. Provided it is demonstrated that the notch can consistently control the fatigue crack location (and not prevent the cylinder

design from achieving the minimum number of pressure cycles required for a 15- to 20-year cylinder life), then the notch shall be applied to all production cylinders. The crack length generated at the notch by pressure cycling to failure shall be used as the machined flaw size. The flaw size shall be machined into the external surface of the cylinder at the location of the notch, and the cylinder hydraulically burst at a pressure greater than 1.25 times the service (working) pressure. The fracture surfaces shall be examined to confirm that the fracture did not extend beyond the machined length of the flaw.

4. For Type 1 steel cylinders, an alternative to the LBB performance test is to use the following parametric equation to calculate the critical flaw size:

$$L_d = 0.00038 \cdot RT^{0.473} \cdot \sigma_y^{2.087} \cdot \left(\frac{J_1}{1000}\right)^{0.446} \cdot \sigma_H^{0.013J_1} \cdot \exp\left[-0.024\sigma_H - 0.008\sigma_y + 0.1\left(\frac{J_0}{1000}\right) - 0.064\left(\frac{J_1}{1000}\right)\right] \quad (1)$$

where L_d is the estimated crack length in inch, R , is the outer radius in inches, T is the wall thickness in inches, σ_y is yield strength in ksi, σ_H is hoop stress in ksi, J_0 resistance curve intercept in in-lb /in² x10³ and J_1 resistance curve slope, in in-lb/in x10³.

Fracture resistance parameters of the material (J_0 and J_1) shall be obtained using ASTM E1152-87 “Standard Test Method for Determining J-R Curves”. Hoop stress shall be calculated using the following equation:

$$\text{hoop stress} = \text{maximum fill pressure (ksi)} \times R/T$$

The acceptance criterion shall be that L_d does not exceed the maximum crack length (as determined from the pressure cycling of the three cylinders to failure) multiplied by 2.

5. For Type 1, Type 2, and Type 3 cylinders, the maximum defect size for NDE inspection can be determined using the following performance test:

- a) A longitudinal flaw shall be machined into the internal sidewall surface of cylinder or liner shells (prior to the end closing operation) using EDM techniques, or a 30° CVN cutter of 3-4 inch (75-101 mm) diameter, thickness of 0.0625 inches (1.6 mm) or less, and a tip radius of 0.010 inch (0.25 mm) or less. The flaw depth shall not be greater than 5% of the wall thickness.

- b) The completed cylinder shall then be pressure cycled to failure from 300 psi (2.07 MPa) to 1.25 times the service (working) pressure to demonstrate the minimum required fatigue (pressure cycle) life can be achieved.

- c) The manufacturer shall demonstrate that the NDE inspection method can detect defects which exceed the maximum defect size.

REFERENCES

1. ISO/DIS 11439: Gas Cylinders – “High Pressure Cylinder for the On-Board Storage of Natural Gas as a Fuel for Automotive Vehicles”.
2. Canadian Standards Association B51: Part 2, “High Pressure Cylinder for the On-Board Storage of Natural Gas as a Fuel for Automotive Vehicles”, CSA B51-97, September 1997.
3. Proposed American National Standard for Basic Requirements for Compressed Natural Gas Vehicle (NGV) Fuel Containers, July 1997.
4. Webster, C., et al., “Life Expectancy of Steel Fuel Cylinders for Natural Gas Vehicles”, Gas Technology Canada, report TP 12910E, for Transportation Development Centre, July 1997.
5. Akhtar, A., et al., “NGV Cylinder Integrity Assessment, Volume 1 – All Steel Cylinders”, Powertech Labs report TP 10829E for Transportation Development Centre, February 1991.
6. Rana, M., et al., “Technical Basis for Flawed Cylinder Test Specification to Assure Adequate Fracture Resistance of ISO High Strength Steel Cylinder”, ASME PVP-Vol. 342, Fatigue and Fracture (Ed. K.K. Koon, et al.), Book No. H01052-1996.
7. Webster, C., “The Development of an Advanced Cylinder for the High Pressure Storage of Compressed Hydrogen and Hythane Fuels”, Powertech Labs report for Natural Resources Canada on Contract No. 23440-5-1340/001/SQ, March 1998.
8. Milne, L., et al., “Assessment of the Integrity of Structures Containing Defects”, Revision 3, CEGB report R/H/Rb-Rev.3, 1985.
9. British Standard, “Transportable Gas Containers – Part 1. Specification for Seamless Steel Gas Containers Above 0.5 Litre Water Capacity”, BS 5045: Part 1: 1982

APPENDIX A Fracture Performance Test Program

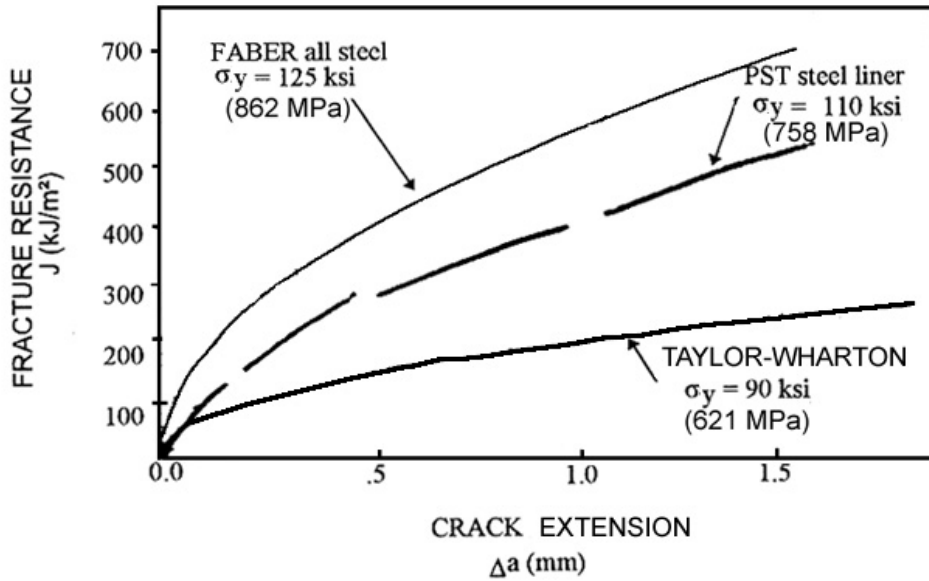
A-1.0 Material Properties of Cylinder Designs

Tensile and fracture properties of Faber and Taylor Wharton all-steel cylinders, Luxfer all-aluminum cylinders (AA7032), Luxfer all-aluminum scuba cylinders (AA6061-T6), Pressed Steel Tank steel liners, and CNG Cylinder Co. aluminum liners were measured using small scale test specimens at room temperature. Fracture properties of the materials were established using the ASTM E813-89[16] fracture toughness test. This test method determines a critical value of “J-integral”, which characterizes the toughness of a material near the onset of crack extension from a pre-existing fatigue crack. The J-integral values were determined from the areas under the load versus load-line displacement curve, obtained from the tests. The tests also produced J-R curves, a plot of J-integral versus ductile crack extension, Δa (as shown in Figures 1 and 2). A critical value of J-integral for the onset of crack initiation, ($J_{0.2}$), defined as the J-integral value corresponding to the intersection of the J-R curve of the material and an offset line drawn at a crack extension (Δa) value of 0.2 mm and having a slope of $(2 \Delta a \sigma_y)$, was obtained for each of the materials. Table A-1 summarizes the measured material properties.

Table A-1. Materials Properties of the Metal Cylinders and the Metal Liners

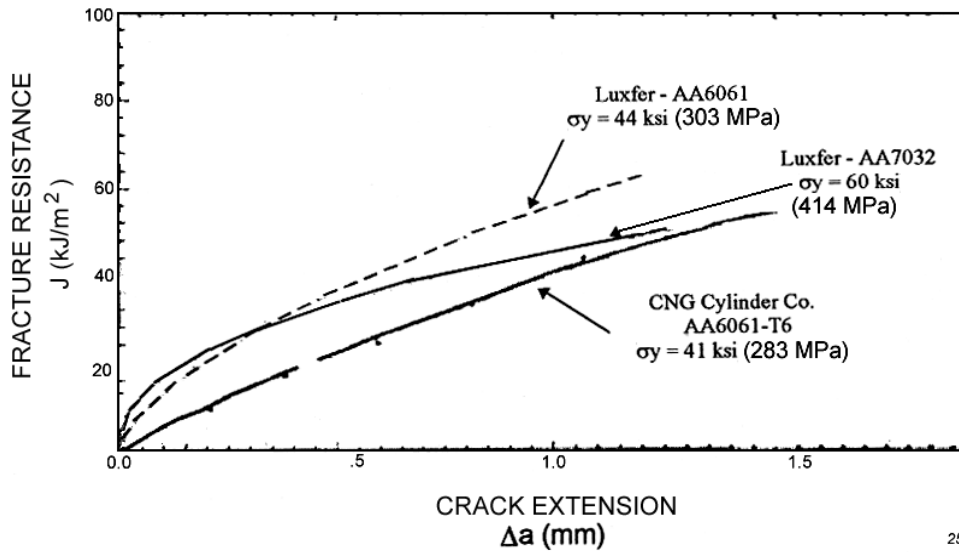
Cylinder/Liner Type	Outside Diameter mm (inch)	Wall Thickness mm (inch)	Average Yield Strength in ksi (MPa)	UTS in ksi (MPa)	Fracture Toughness ($J_{0.2}$) in in-lb/in ² (kJ/m ²)
Faber (steel) cylinder	316 (12.44)	8.2 (0.322)	125 (860)	139 (957)	1428 (250)
Taylor Wharton (steel) cylinder	238 (9.35)	7.11 (0.280)	90 (618)	110 (760)	491 (86)
Luxfer (AA7032 aluminum) cylinder	248 (9.75)	13.3 (0.522)	60 (412)	71 (489)	143 (25)
Luxfer (AA6061 aluminum) cylinder	202 (8)	15.2 (0.599)	44 (300)	48 (330)	126 (22)
Pressed Steel Tank (steel) liner	340 (13.4)	5.8 (0.228)	111 (762)	123 (850)	976 (171)
CNG Cylinder (aluminum) liner	267 (10.5)	11.3 (0.445)	41 (282)	48 (331)	57 (10)

Figures A-1 and A-2 show the fracture resistance material properties (J-R curve) for the all-steel cylinder and the steel liner, and for the all-aluminum cylinder and the aluminum liner, respectively. Note the shape of the J-R curves shown in Figure 1. The curve for the Faber all-steel cylinder material is steeper than that of the Taylor-Wharton cylinder material, reflecting a tougher steel.



25n-1

Figure A-1: Fracture resistance of the steels of Type 1 cylinders and the Type 2 liner.



25o-1

Figure A-2: Fracture resistance of the aluminum Type 1 cylinders and the Type 2 liner.

A-2.0 LBB PERFORMANCE (FLAWED CYLINDER BURST TESTS)

A-2.1 Background

Flawed cylinder burst tests were carried out on all-steel Type 1 and metal-lined Type 2 cylinders. These tests were designed to determine the maximum flaw length that would cause a leak for a particular design at a hydraulic pressure of 125% of the service pressure, and to evaluate the effect of pneumatic pressurization on the failure behaviour of a design containing such a flaw. The flawed cylinders were pressurized to failure using either water or compressed nitrogen.

Flawed burst tests were conducted on the following cylinders:

- Type 1 steel (Faber) cylinders with a service pressure (P_s) of 3,000 psi (20.7 MPa)
- Type 1 steel (Taylor Wharton) with a P_s of 2,400 psi (16.5 MPa)
- Type 1 aluminum (Luxfer) AA7032 cylinders with a P_s of 3,000 psi (20.7 MPa)
- Type 1 aluminum (Luxfer) AA6061-T6 scuba cylinders with a P_s of 3,200 psi (22.0 MPa)
- Type 2 steel lined hoop-wrapped (Pressed Steel Tank) cylinders with a P_s of 3,000 psi (20.7 MPa)
- Type 2 aluminum-lined hoop-wrapped (CNG Cylinder Co.) cylinders with a P_s of 3000 psi (20.7 MPa)

For Type 1 all-metal cylinder designs (excluding the all-aluminum AA7032 design) external axial flaws of varying lengths and having depths of 60% to 95% of the wall thickness were machined onto the external surface in the cylindrical portion of the cylinders using a Charpy V-Notch (CVN) cutting tool. Key parameters for the machined flaws are shown in Figure A-3. Diameter, thickness and angle of the cutter was 3 - 4 inch (76-101 mm), 0.06 inch (1.6 mm), and 30°, respectively. The tip radius of the cutter was 0.010 inch (0.25 mm).

Figures A-4 and A-5 show the shape of a typical axial machined flaw introduced on the surface of an all-steel (Faber) and an all-aluminum (Luxfer) AA6061-T6 cylinder. The all-aluminum AA7032 design has an existing manufacturing notch with an approximate length of 0.75 inch (19 mm) and a depth of 0.025 inch (0.6 mm) machined into the bottom of the cylinder (as shown in Figure A-6), to intentionally force the fatigue crack to initiate at the notch site, as well as to control the size of the final fatigue crack length which would cause eventual failure of the design. For the flawed cylinder burst testing of this particular design, the existing manufacturing

notch at the bottom was extended by machining using a CVN cutter. Figure A-7 shows the cross section of a machined defect at the bottom of an all-aluminum AA7032 Luxfer cylinder.

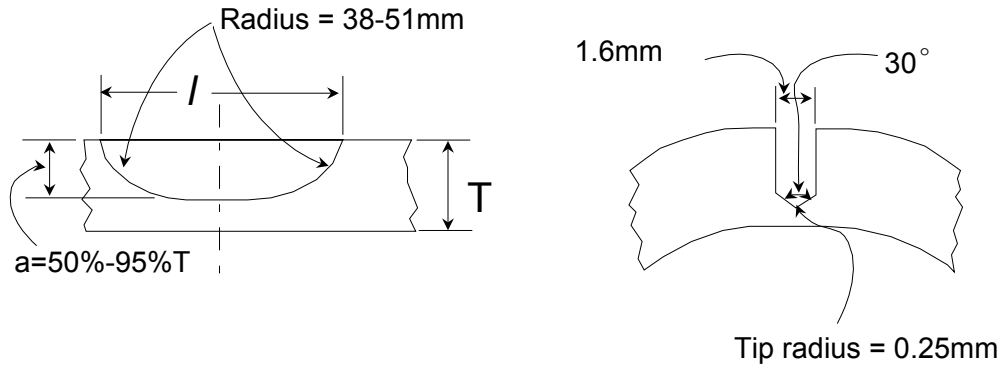


Figure A-3. Key parameter for the flaws machined onto the external surface of the cylinder using CVN cutter.



Figure A-4. Photograph shows location and cross section of machined flaw introduced onto the external surface of an all-steel Faber cylinder.



Figure A-5. Photograph shows cross section of an axial external machined flaw introduced onto.

For Type 2 hoop-wrapped designs, deep axial defects were introduced onto the outer surface using the CVN cutter with a 30° angle. Cuts were made through the entire hoop wrap composite and extending into 80% of the liner wall. Figure A-8 shows a typical machined flaw for an aluminum hoop-wrapped cylinder.

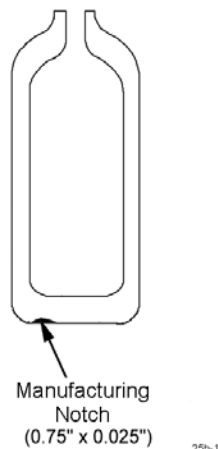


Figure A-6. Schematic of an all-aluminum (AA7032) Luxfer cylinder, showing the location of the manufacturing notch.

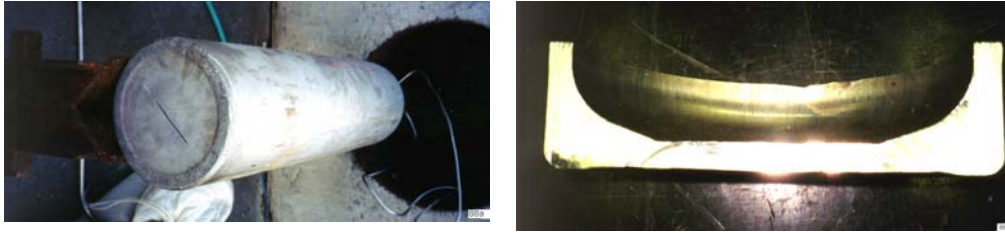


Figure A-7. Photograph shows location and shape of the external defect, machined onto the bottom of an all-aluminum (AA7032) Luxfer cylinder.

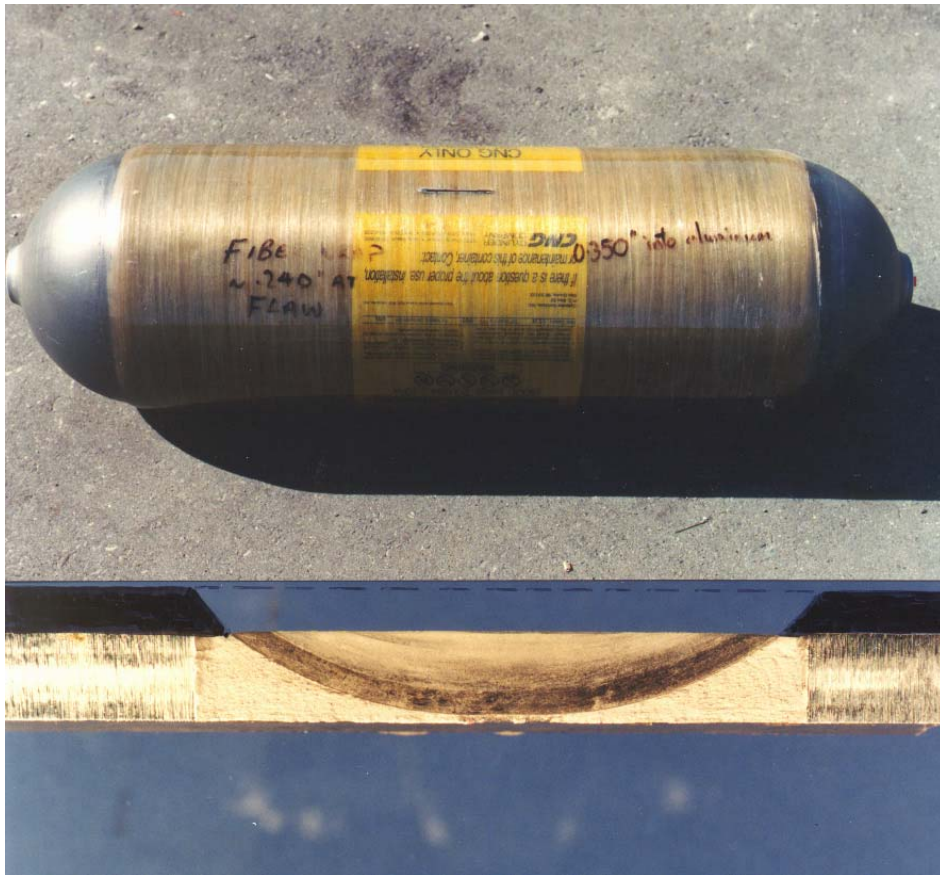


Figure A-8. Photograph showing location and cross section of a machined flaw introduced onto the external surface of an aluminum-lined hoop-wrapped (CNG Cylinder Co.) cylinder.

A-2.2 LBB Test Results

A-2.2.1 All-Metal (Type 1) Cylinders

The results of pneumatic and hydraulic bursts of steel and aluminum cylinders containing external flaws are presented in Tables A-2 and A-3.

Table A-2: Summary of Flawed Cylinder Burst Test Results - All-steel Cylinders

Cylinder Type	Flaw length (times wall thickness T)	Flaw depth (% of wall thickness, T)	Medium of Pressurization	Failure Pressure, psi (MPa)	Failure mode
Faber	10.2T	80%T	hydraulic	3,750 (25.9)	leak
Faber	10.0T	80%T	pneumatic	3,700 (25.5)	leak
Faber	12.4T	80%T	pneumatic	3,220 (22.2)	leak
Taylor Wharton (long length)	4.0T	80%T	hydraulic	4,962 (34.2)	rupture
Taylor Wharton (long length)	10.0T	60% T	hydraulic	3,700 (25.5)	rupture
Taylor Wharton (long length)	10.0T	70% T	hydraulic	3,100 (21.4)	leak
Taylor Wharton (long length)	10.0T	83%T	hydraulic	3,190 (22.0)	leak
Taylor Wharton (long length)	10.0T	80%T	pneumatic	3,200 (22.1)	rupture
Taylor Wharton (short length)	10.0T	84%T	hydraulic	3,146 (21.7)	leak
Taylor Wharton (short length)	10.0T	90%T	pneumatic	2,830 (19.5)	leak

Table A-3: Summary of Flawed Cylinder Burst Test Results - All-Aluminum Cylinders

Cylinder Type	Flaw Length (times the wall thickness T)	Flaw Depth (% of wall thickness, T)	Medium of Pressurization	Failure Pressure, psi (MPa)	Failure mode
Luxfer AA6061-T6	4.0T	80%T	hydraulic	5,660 (39.0)	rupture
Luxfer AA6061-T6	6.0T	80%T	hydraulic	4,040 (27.9)	leak
Luxfer AA6061-T6	10.0T	60%T	hydraulic	3,910 (27.0)	fracture
Luxfer AA6061-T6	10.0T	70%T	hydraulic	3,240 (22.3)	fracture
Luxfer AA6061-T6	6.0T	80%T	pneumatic	3,910 (27.0)	rupture
Luxfer AA6061-T6	5.0T	95%T	pneumatic	3,480 (24.0)	leak
Luxfer AA6061-T6	4.0T	98%T	pneumatic	3,980 (27.4)	leak
Luxfer AA7032*	9.4T	99%T	pneumatic	2,200 (15)	leak

* Machined flaw cut into the manufacturing notch at the bottom. "T" is the thickness of the AA7032 cylinder at the bottom.

A Faber steel cylinder with a 3.3 inch (84 mm) long axial flaw having a depth of approximately 80% of wall thickness leaked under a hydraulic pressure of 3,750 psi (25.85 MPa) as shown in Figure A-9. There was no extension (tearing) of the flaw beyond the original machined length. This type of failure is defined as the *leak failure mode*.

One of the long Taylor Wharton cylinders containing a 1 inch (25 mm) long flaw having a depth of 80% of wall thickness failed at a hydraulic pressure of 4,962 psi (34.2 MPa), which is twice the service pressure. It exhibited significant bulging near the failure location, as shown in Figure A-10a. The bulging is associated with ductile tearing of the machined flaw. This type of failure is defined in this report as the *rupture failure mode*.

An all-aluminum (AA6061-T6) cylinder having a service pressure of 3,200 psi (22 MPa) and containing a 2.4 inch (61 mm) long axial defect having a depth equal to 80% of the wall thickness ruptured at a hydraulic pressure of 175% of the service pressure (as shown in Figure A-10b). For some of the flawed burst tests on the aluminum cylinders, the machined flaw cracked along the axial direction for more than 10% of the original length of the flaw without causing significant localized bulging in the failed cylinder (as shown in Figure A-11). This type of failure is defined in this report as the *fracture failure mode*.



Figure A-9. An all-steel Faber cylinder with a 3.3" (84 mm) long axial flaw having a depth of approximately 80% of wall thickness leaked under a hydraulic pressure of 3,750 psi (25.85 MPa)



(a)



(b)

Figure A-10: Rupture failure mode of flawed all-metal cylinders tested in hydraulic conditions:

- (a) all-steel Taylor Wharton (long)*
- (b) all-aluminum Luxfer scuba cylinder*



Figure A-11. Figures show the extension of the machined flaw along the length of the all-aluminum (AA6061-T6) Luxfer cylinders, observed during the hydraulic flawed cylinder burst tests:
(a) cylinder having a flaw (9.6T long and 67%T deep) failed at 3,240 psi (22.3 MPa)
(b) cylinder having a flaw (9.6T long and 57%T deep) failed at 3,910 psi (27.0 MPa).

An all-steel Faber cylinder with an external flaw 10 times longer than the wall thickness (T) and having a depth of 80% of the wall thickness leaked at a pneumatic pressure of 3,700 psi (25.5 MPa), or 123% of the service pressure. A long length Taylor Wharton cylinder with a 10T long axial flaw and a depth equal to 80% of the wall thickness ruptured under pneumatic pressurization at an internal pressure of 133% of the service pressure (shown in Figure A-12b). Another long Taylor Wharton cylinder with a similar flaw size leaked under hydraulic pressurization at a similar failure pressure (shown in Figure A-12a). It should be noted that yield strength and fracture toughness of the Taylor Wharton cylinder materials were approximately 71% and 59%, respectively, of the Faber steel cylinder material (refer to Table A-1).

An all-aluminum (AA6061-T6) cylinder with a 3.6 inch (91 mm) (5.9 T) long axial external flaw having a depth of 0.48 inch (12.2 mm) (79% of the wall thickness) ruptured into two pieces at a pneumatic pressure of 3,910 psi (27.0 MPa), as shown in Figure A-13b. Note that another cylinder from the same design (shown in Figure A-13a) with a similar flaw leaked at a hydraulic pressure of 4,040 psi (27.85 MPa).

Cylinder test data such as flaw length, failure pressure/service pressure (P_f/P_s), and mode of failure, as obtained from the flawed burst tests conducted in hydraulic as well as in pneumatic condition, are plotted in Figure A-14 for the all-steel designs. Previous test data obtained from cyclic as well as flawed burst tests on Faber all-steel cylinders are also included*.

A solid curve representing the upper boundary of the observed leak failure mode data for the all-steel NGV cylinders is drawn in Figure A-14. This solid curve represents the transition from leak to rupture of the all-steel NGV cylinders. It can be seen that an axial flaw having a length less than 10-13 T would cause a leak of an all-steel NGV cylinder at a failure pressure of 125% of the service pressure. Average test data, as obtained by the ISO WG14 from tests on all-steel industrial gas cylinders**, are also shown as a dotted line in Figure A-14 for comparison. Better fracture performance is evident from this figure for all-steel NGV cylinders as compared to all-steel industrial gas cylinders. This better fracture performance may be attributed to the much tougher material of the Faber cylinders.

* Bhuyan, G., et al, "Integrity of On-Board and Ground Storage NGV Cylinders", Proc. of 2nd IANGV Conference, 1990.

** Rana, M., et al, "Technical Basis for Flawed Cylinder Test Specification to Assure Adequate Fracture Resistance of ISO High Strength Steel Cylinder", Proc. of the 1996 ASME PVP Conference, Montreal.

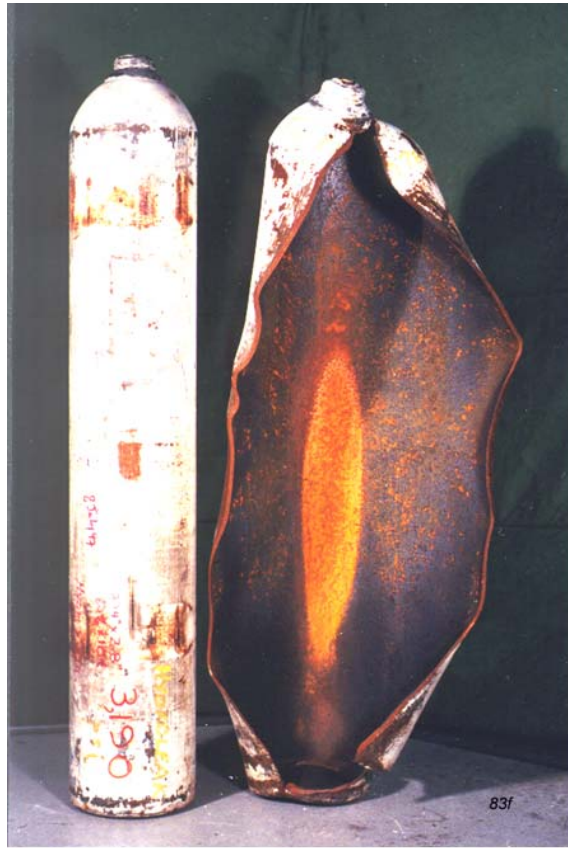


Figure A-12. Effect of medium of pressurization on the failure mode of long all-steel Taylor Wharton containing a 10T long machined flaw:
(a) cylinder having a flaw 83%T deep leaked under hydraulic pressurization
(b) cylinder having a flaw 80%T deep ruptured under pneumatic pressurization

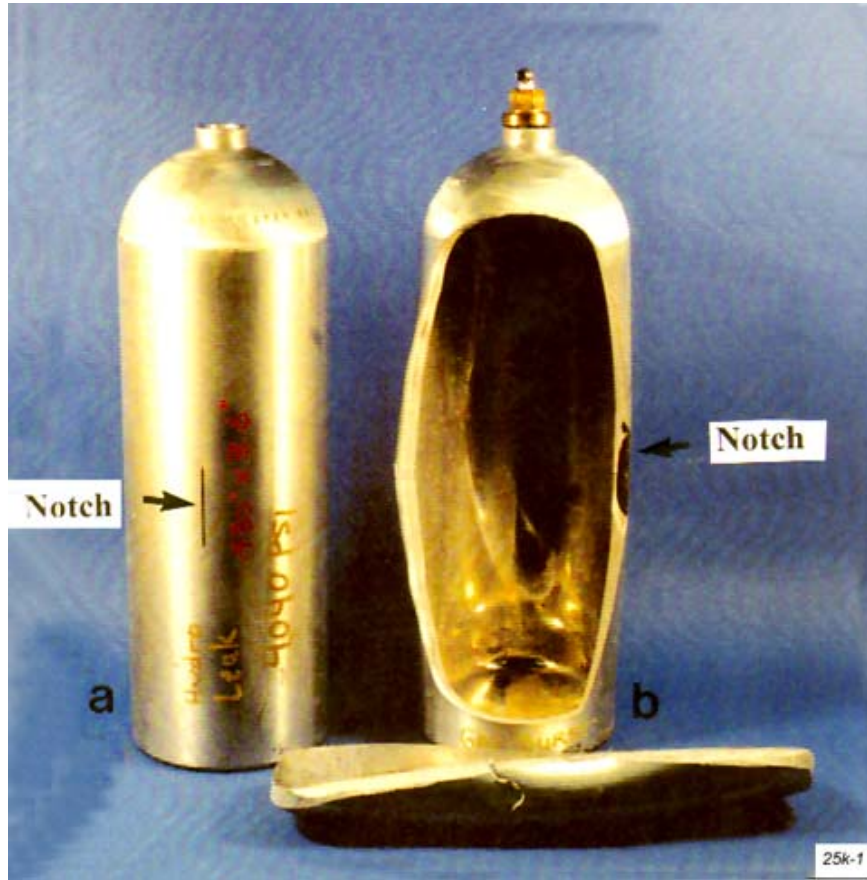


Figure A-13. Effect of medium of pressurization on failure mode of all-aluminum (AA6061-T6) Luxfer cylinders containing 6T long and 80%T deep axial external machined flaw:
(a) cylinder leaked under hydraulic pressurization
(b) cylinder ruptured under pneumatic pressure.

Flawed cylinder burst test data on all-aluminum (AA6061-T6) cylinders (shown in Table A-3) are plotted in Figure A-15. A transition curve has been drawn to separate the general leak failure zone from the rupture failure zone. It can be seen that an axial flaw length of greater than five times the wall thickness would tend to cause rupture of the design at a pressure equivalent to 125% of the service pressure.

The Luxfer all-aluminum (AA7032) NGV cylinders, containing a 5T long defect grown from the manufacturing notch in the base of the cylinder, would leak in hydraulic pressurization. Flaw tolerance of this design in pneumatic pressurization could not be established from the present program.

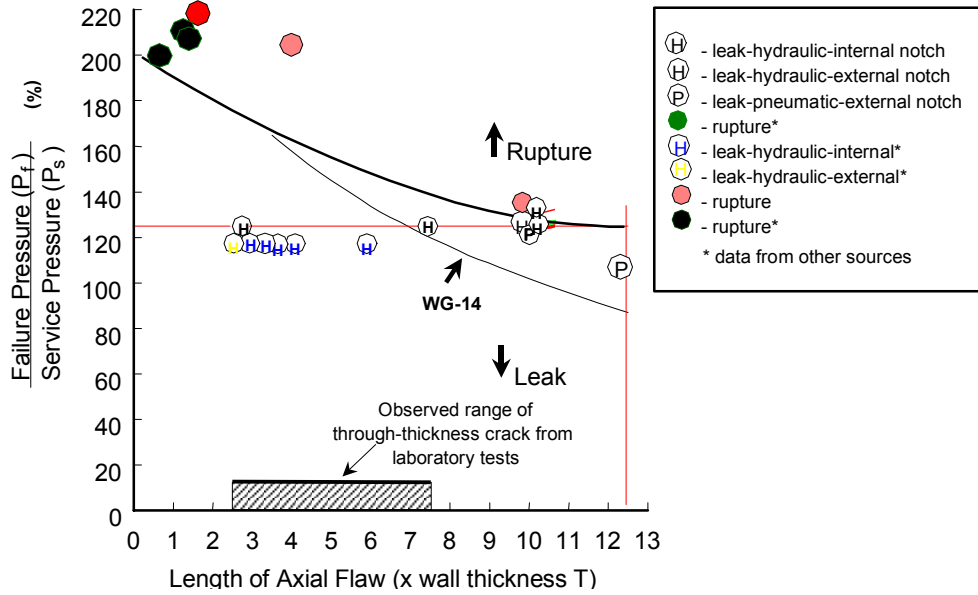


Figure A-14: Flaw tolerance of all-steel NGV cylinders

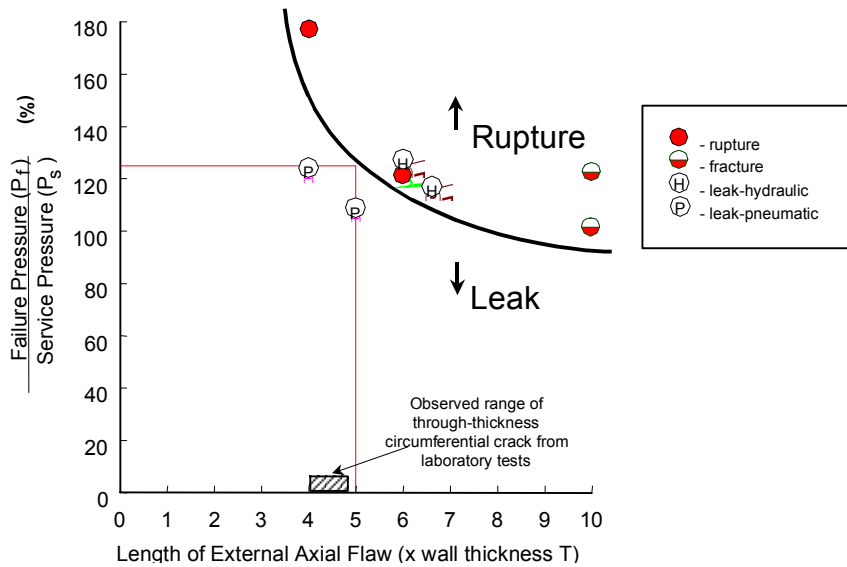


Figure A-15: Flaw tolerance of all-aluminum (AA6061-T6) cylinders

During hydraulic flawed cylinder burst tests it was observed that internal pressure dropped quickly in the event of the defect becoming a through-wall crack. During the pneumatic flawed cylinder burst tests, on the other hand, the rate of pressure drop was not significant compared to that of the hydraulic test. The faster drop of hydraulic pressure in the event of a through-wall defect is due to the incompressible nature of water. As a result, only a relatively small loss is required to effect a significant change in pressure. In the event of a leak in hydraulic pressurization, the extended defect is therefore subjected to a lower pressure resulting in no significant increase in crack driving force. However, in the event of a pneumatic pressurization, the extended defect is subjected to a higher crack driving force for a longer period of time, which could cause instability if the tearing resistance of the material is relatively low. This may explain why the flawed cylinders failed catastrophically in pneumatic pressurization, as shown in Figure A-12b and A-13b, and not catastrophically in hydraulic pressurization, as shown in Figure A-10.

The above scenario probably also applies to aluminum cylinders. For example, an all-aluminum cylinder shown in Figure A-13a leaked in hydraulic pressurization. Another cylinder with a similar crack, pressurised with air, ruptured into three pieces, as shown in Figure A-13b. Although the cylinder leaked under hydraulic pressurization, ductile tearing was evident from the machined notch during the test. The extent of tearing around the machined notch during hydraulic pressurization testing of the flawed cylinder is shown in Figure A-16, along with the fractured surface of the leak. Maximum tearing of 5.7% beyond the length of the machined flaw was observed.

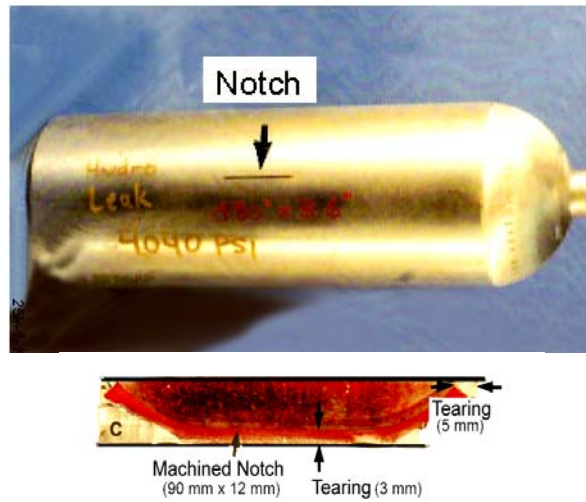


Figure A-16. Fracture surface of an all-aluminum (AA6061-T6) cylinder leaked under hydraulic pressurization. Photograph shows the ductile tearing of the machined defect during the hydraulic burst test.

A.2.2.2 Hoop-Wrapped (Type 2) Cylinders

Flawed cylinder burst tests carried out on the hoop-wrapped designs simulated damage of the composite wrap under the mounting strap, and the eventual growth of a fatigue crack in the liner under the wrap damage. Since the width of the strap damage is about 2 inches (51 mm), defects greater or equal to 2 inches (51 mm) long were cut through the entire composite and into over 80% of the liner wall thickness. The results of pneumatic and hydraulic bursts on steel hoop-wrapped and aluminum hoop-wrapped cylinders containing external flaws, as well as the results of pressure cycling undamaged hoop-wrapped cylinders to failure, are presented in Table A-4.

Table A-4: Summary of Flawed Cylinder Burst & Cycle Test Results – Hoop-Wrapped Designs

Cylinder Type	Flaw Length measured on cylinder, in inches (mm)	Flaw Length measured on the liner, in inches (mm)	Flaw depth in the liner (% of liner thickness, t)	Medium of Pressurization	Failure Pressure P_f / Service Pressure P_s	Failure mode
Steel hoop wrap	3.25 (83)	2.2 (56)	86%t	hydraulic burst	1.19	leak
Steel hoop wrap	3.25 (83)	2.2 (56)	78%t	pneumatic burst	0.87	leak
Steel hoop wrap	2.0 (51)	1.8 (46)	95%t	pneumatic burst	1.10	leak
Steel hoop wrap	2.0 (51)	-	100%t	hydraulic cycling	1.25	leak
Steel hoop wrap	-	0.7 (18)	100%t	hydraulic cycling	1.25	leak
Aluminum hoop wrap	4.4 (112)	3.9 (99)	83%t	hydraulic burst	0.69	leak
Aluminum hoop wrap	3.1 (79)	2.7 (69)	92%t	hydraulic burst	0.78	leak
Aluminum hoop wrap	2.4 (61)	2.0 (51)	85%t	hydraulic burst	1.24	leak
Aluminum hoop wrap	2.8 (71)	2.3 (58)	84%t	pneumatic burst	1.13	leak
Aluminum hoop wrap	-	1.9 (48)	100%t	hydraulic cycling	1.25	leak
Aluminum hoop wrap	-	1.0 (25)	100%t	hydraulic cycling	1.25	leak
Aluminum* hoop wrap	-	4.0 (102)	95%t	pneumatic burst	1.67	leak

*External machined flaw introduced at the neck area, “t” is the liner thickness at the neck area

The steel hoop-wrapped cylinder with a 3.25 inch (82.6 mm) long flaw having a depth extending to 90% of the liner thickness leaked at a pressure of 3,560 psi (24.5 MPa). An aluminum-lined hoop-wrapped cylinder with a 2.4 inch (60 mm) long axial machined cut through the entire composite thickness and into 83% of the liner thickness leaked at an internal pressure of 3,730 psi (25.7 MPa).

A steel-lined hoop-wrapped cylinder containing a 3.25 inch (83 mm) long machined cut through the entire composite and extending into 95% of the liner thickness leaked at a pneumatic pressure of 3,293 psi (22.7 MPa), as shown in Figure A-17a. An aluminum-lined hoop-wrapped cylinder containing a 2.8 inch (71mm) long machined cut through the entire composite and extending into 84% of the liner wall leaked at a pneumatic pressure of 3,410 psi (23.5 MPa), as shown in Figure A-17b.



(a)



(b)

Figure A-17. Photographs show leak failure mode of hoop-wrapped design after pneumatic pressurization: (a) a PST cylinder containing a 2 inch (51 mm) long axial defect extending to 95% of the liner failed at 3,293 psi (22.7 MPa) (b) a CNG Cylinder Co. cylinder, containing a 2.8 inch (71 mm) long defect extending to 84% of the liner thickness leaked at 3,410 psi (23.5 MPa).

An external defect was machined at the neck area of an aluminum hoop-wrapped cylinder, as shown in Figure A-18. The cylinder, which contained a 4 inch (101 mm) long flaw having a depth of 95% of the neck thickness, leaked at a pneumatic pressure of 167% of service pressure. The flawed cylinder test data under pneumatic conditions demonstrates that the hoop-wrapped designs would leak at the maximum fill pressure, provided that the hoop-wrap is not significantly damaged. In the event of fatigue cracking in the neck/head region, an area not supported by the composite, the design demonstrated a safe failure mode at the maximum fill pressure.

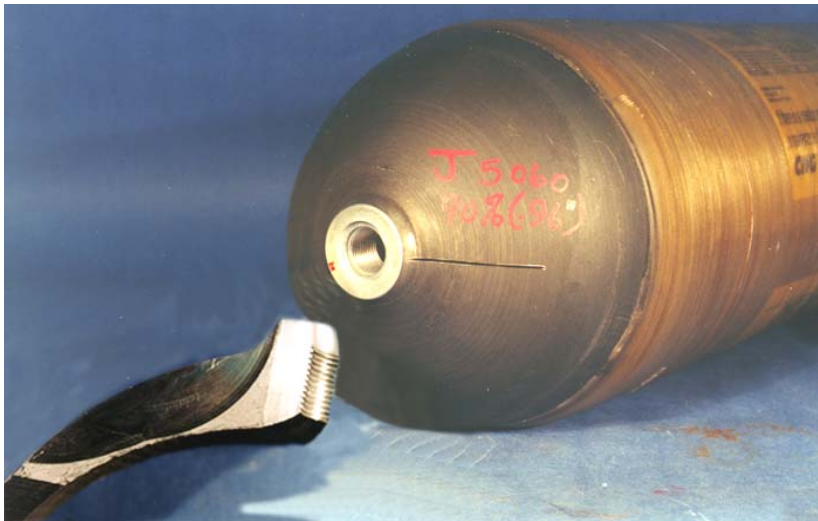


Figure A-18. Photograph shows the location and shape of the external machined flaw (4.0" long [101 mm] and 95% of the neck thickness) introduced onto the neck/shoulder region of an aluminum-lined hoop-wrapped CNG Cylinder Co. cylinder. The cylinder leaked under pneumatic pressurization.

A-2.2.3 LBB Pressure Cycling Tests

Cylinders either with or without machined defects were pressure cycled from 300 psi to 3,750 psi (2 MPa - 25.85 MPa) using water. Machined defects were introduced either onto the external surface or onto the internal surface of the cylinders.

Pressure cycling tests were carried out on the following cylinders:

- all-steel cylinders (Faber)
- all-aluminum AA7032 cylinders (Luxfer)
- all-aluminum AA6061-T6 scuba cylinders (Luxfer)
- steel-lined hoop-wrapped cylinders (PST)
- aluminum-lined hoop-wrapped cylinders (CNG Cyl. Co.)

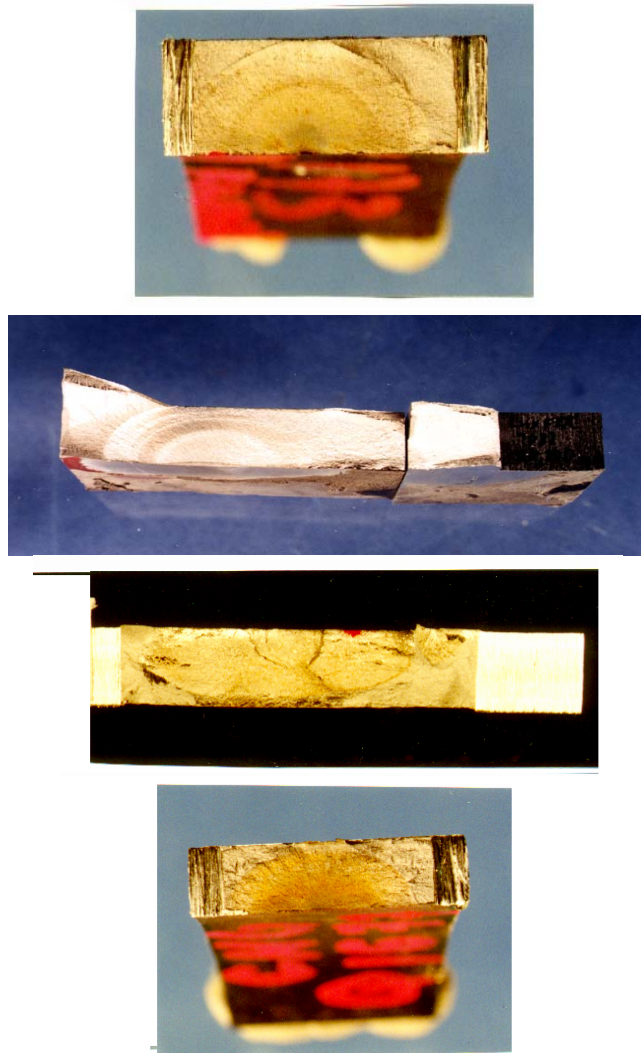
Cylinders of all-steel, all-aluminum, steel-lined hoop-wrapped and aluminum-lined hoop-wrapped designs without any machined defects were pressure cycled to failure. A few all-aluminum cylinders manufactured from AA7032 alloy and containing intentional external manufacturing notches at the base were also pressure cycled. (Note: These notches are part of the Luxfer manufacturing process for this particular cylinder type.) The total number of cycles, the length of the leak and the location of failure for the tested cylinders are summarized in Table A-5. All of the tested cylinders failed by leakage rather than from rupture. The number of fatigue cycles exceeded the minimum number required for NGV service.

Table A-5. Fatigue Life and Length of Through-Thickness Fatigue Crack for Various Designs

Cylinder Type	Number of fatigue cycles to failure	Length of the through-thickness fatigue crack, in terms of thickness of wall (T) or liner (t) at the crack location	Failure Mode using Hydraulic pressurization	Location/orientation of the fatigue failure
Faber all steel	45,075	2.7 T	leak	midsection/axial
Luxfer AA7032	20,200	5.0 T	leak	manufacturing notch at the bottom
Luxfer AA6061-T6	58,297	4.6 T	leak	bottom knuckle/circumferential
Luxfer AA6061-T6	43,250	3.9 T	leak	bottom knuckle/circumferential
CNG Cylinder Co.-aluminum hoop wrap	55,980	4.3 t	leak	midsection/axial
CNG Cylinder Co.-aluminum hoop wrap	27,370	2.2 t	leak	midsection/axial
PST -steel hoop wrap	24,620	2.9t	leak	midsection/axial

Shapes of the observed through-wall fatigue cracks in the all-steel Faber, all-aluminum Luxfer AA7032, and hoop-wrapped cylinders (CNG Cyl. Co. and PST) are shown in Figure A-19. Note the elliptical shape of the through wall fatigue cracks. Fatigue cracks grew from the manufacturing notch (Figure A-19b) of the all-aluminum AA7032 cylinder and became a leak after 20,200 cycles. A fatigue crack (Figure A-19c) initiated from the outer surface of the liner of the aluminum hoop-wrapped cylinder and became a leak after 55,980 cycles.

Location and shape of the circumferential fatigue cracking observed for the all-aluminum AA6061-T6 cylinders with flat bottoms are shown in Figure A-20. Even though the internal surface of one of the AA6061-T6 cylinders was scratched prior to cycling, having a depth of approximately 0.01 inch (0.3 mm) at the midsection, the fatigue crack initiated at the bottom of the knuckle and caused a leak after 43,250 cycles under hydraulic pressurization.



*Figure A-19. Photograph shows size and shape of leak observed during fatigue cycling of the cylinders.
(a) all-steel (Faber)
(b) all-aluminum (Luxfer AA7032)
(c) aluminum lined hoop-wrapped (CNG Cylinder Co.)*



(a)



(b)



(c)

Figure A-20. Photograph shows location, orientation and size of the fatigue crack, causing leak of an all-aluminum (Luxfer AA6061-T6) cylinder in hydraulic pressurization.

- (a) location of the leak,
- (b) orientation of the crack,
- (c) shape and size of the leak.

In one of the aluminum hoop-wrapped cylinders pressure cycled to failure, internal defects were introduced by cold chiselling at the neck area on aluminum hoop-wrapped cylinders (as shown in Figure A-21). The chiselled defects were 1.5 inch (38 mm) long and 0.2 inch (5 mm) deep. However, a fatigue crack was initiated at the mid section and became a leak after 27,370 cycles.



Figure A-21. Photograph shows the location of an internal gouge mark (1.5 inch [38 mm] long and 0.2 inch [5 mm] deep) introduced at the neck area of an aluminum-lined hoop-wrap CNG Cylinder Co. cylinder by cold chiselling method prior to fatigue cycling.

A-3.0 NDE DEFECT SIZE (FLAWED CYLINDER PRESSURE CYCLING)

A-3.1 Effect of Defect Location

Four 10T long axial defects, having a depth of 6%T to 13%T (see Table A-7), were introduced onto external and internal surfaces of an all-steel cylinder using the electro discharge machining (EDM) technique. The neck region of the cylinder was modified as shown in Figure A-22a in order to introduce internal EDM defects. Locations of these EDM cuts are shown in Figure A-22b. The cylinder with these four EDM defects was cycled from 300 psi (2 MPa) to 3,750 psi (25.85 MPa) using water. Growth of cracks from these initial external EDM defects was monitored periodically using eddy current methods, while growth of cracks from internal EDM defects was monitored using ultrasonic test methods. After 5,000 pressure cycles a crack was initiated only from the deeper (9%T) internal defect. NDE measurements after 10,000 pressure cycles indicated crack growth from the remaining three initial EDM defects. However, a fatigue crack initiated from the shallower internal EDM defect (6%T) at a later stage became a leak after 15,647 cycles. The shape of the EDM defect which caused the leak is shown in Figure A-22c.

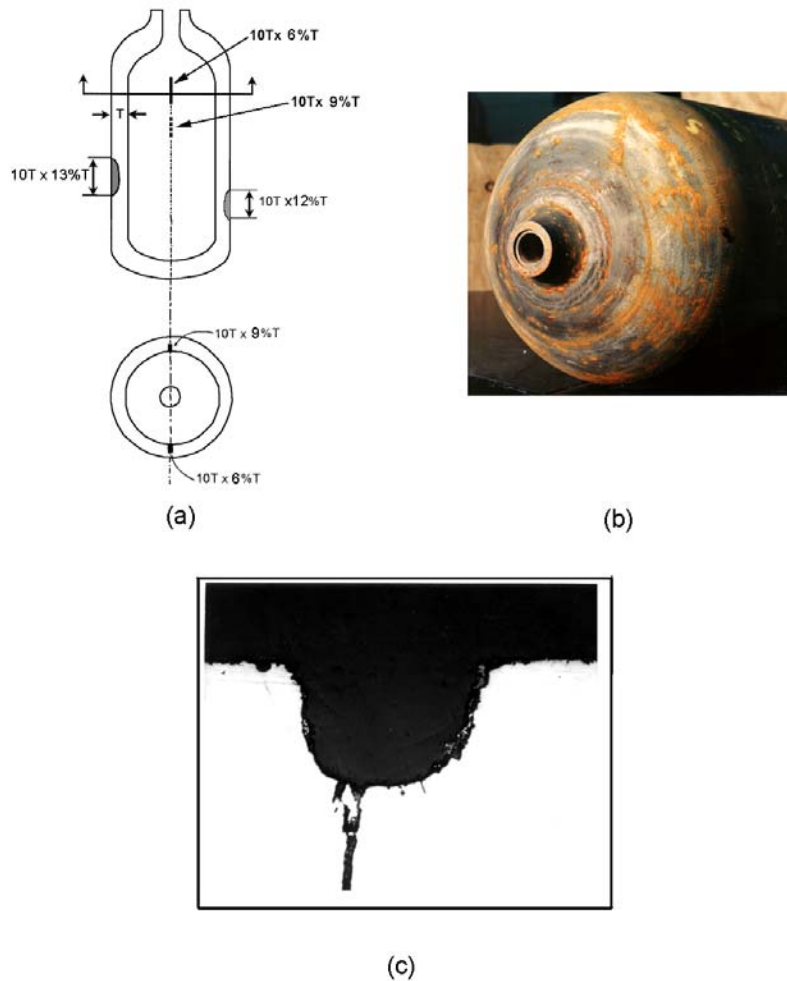


Figure A-22. Faber all-steel cylinder with internal and external EDM flaws:

- (a) location of EDM cuts,
- (b) neck region rewelded after introduction of internal defects.
- (c) shape of the internal EDM defect at which the leak occurred due to fatigue crack growth

A-3.2 Effect of Defect Machining Method

To investigate the effect on cylinder fatigue life of various machining techniques for introducing defects, 2.0 to 2.5 inch (51 to 63 mm) long axial defects were machined onto one Faber all-steel and one Luxfer all-aluminum AA6061-T6 cylinder. The depth of the defects was 3-6% of the wall thickness. In all, four different defects (except scribing) were introduced onto the steel cylinder and five onto the aluminum cylinder, using the following machining techniques:

- grinding wheel
- a 30° CVN cutter
- a 45° CVN cutter
- EDM technique
- scribing (scratching)

The shapes of various 2 to 2.5 inch (51 to 64 mm) long and 3 to 6% deep defects introduced onto the external surface of all-steel and an all-aluminum cylinder are shown in Figures A-23 and A-24, respectively. Growths of machined flaws due to pressure cycling of cylinders are summarized in Table A-7. In the all-steel cylinder, fatigue crack growth from the defect introduced by a 30° CVN cutter caused a leak. The defect introduced by grinding grew to 30% of the wall, whereas the two other defects (EDM and 45° cutter) had a growth less than 18% of the wall thickness. In the all-aluminum cylinder, a fatigue crack initiated from the EDM defect became a leak. The 30° CVN defect grew to a depth of 26% of the wall thickness. The other three defects (introduced by grinding, scribing and the 45° cutter) essentially did not grow during the fatigue cycles. Fracture shape of the leak of the all-steel cylinder is shown in Figure-23e. It can be seen from Figures A-23 and A-24 that shapes of the defects machined by EDM and a 30° CVN cutter are similar.

Fatigue crack growth from the 3 to 6% deep defects introduced by various machining techniques were monitored using eddy currents. Depth of the machined defects and final depth of the extended defects at the end of pressure cycling of the cylinders were compared with that of the eddy current measurements. Based on the comparison, the NDE measurements were calibrated accordingly. The calibrated fatigue crack growths are shown in Figures A-25 and A-26 for the all-steel and the all-aluminum cylinders.

Fatigue crack growths from EDM defects machined onto both the internal and external surface of an all-steel cylinder were monitored using ultrasonic and eddy current method, respectively. The NDE measurements were calibrated by comparing with the actual depths prior to and at the end of pressure cycling of the cylinder. Calibrated fatigue crack growths from 6 to 9% deep EDM defects introduced onto the internal surface are compared in Figure A-30 with 12 to 13% deep external EDM defects. It should be noted that a fatigue crack was first initiated from the internal 9% deep crack. Using crack driving force solutions^{***}, it was found that internal axial semi-elliptical cracks having a depth of 10% of the wall thickness of an all-metal cylinder have higher crack driving forces than external flaws. This could be the reason that the fatigue crack initiated from the internal defect. However, due to the autofrettage process as well as complex

*** Zahoor, A., Ductile Fracture Handbook, 1990

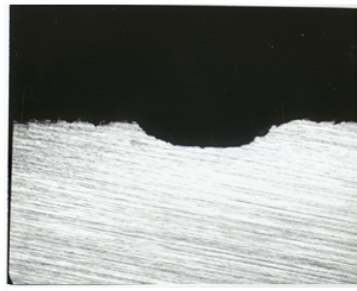
load sharing between metal liner and composite, effect of a shallow defect machined onto external surface of the liner of a Type 2 or a Type 3 on fatigue behaviour could not be assessed.

The presence of a 2 inch (51 mm) long machined flaw, cut through the entire composite and extending into 5% of the liner wall thickness of the steel-lined hoop-wrapped cylinder, caused a remaining fatigue life of 19,469 cycles. A 2 inch (51 mm) long machined flaw cut through the entire composite wrap and extending into 5% of the liner thickness of the aluminum-lined hoop-wrapped cylinder reduced the fatigue life of the cylinder to 8,036 cycles. This result indicates that cutting through the composite wrap to produce an external flaw of less than 2 inches (51 mm) length in the metal liner will have an effect on the cylinder fatigue life.

Table A-7. Growth of Machined Flaws Due to Pressure Cycling of Cylinders from 300 to 3,750 psi [2 - 25.85 MPa] Using Water

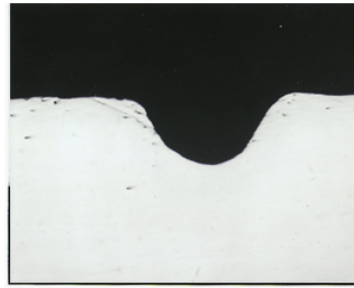
Cylinder Type	Machining Technique	Location	Initial defect length, in inch (mm)	Initial Defect depth, in % of wall thickness(T) or liner thickness(t)	Number of fatigue cycles	Depth of the flaw at the end of fatigue cycles, in % of wall/liner thickness
Faber all-steel	grinding	External	2.5(64)	4%T	32,721	30%T
	30° cutter	External	2.4(61)	5%T	32,721	100%T
	45° Cutter	External	2.4(60)	5%T	32,721	18%T
	EDM	External	2.0(51)	6%T	32,721	16%T
Luxfer - all-aluminum (AA6061)	scratch grinding	External	2.0(51)	3%T	60,946	3% T
	30° cutter	External	2.0(51)	5%T	60,946	6% T
	45° cutter	External	2.0(51)	6%T	60,946	26% T
	EDM	External	2.0(51)	5%T	60,946	5%T
	EDM	External	2.0(51)	5%T	60,946	100%T
Faber - all-steel	EDM	External	3.2(81)	12%T	15,647	16%T
	EDM	External	3.2(81)	13%T	15,647	48%T
	EDM	Internal	3.2(81)	9%T	15,647	55%T
	EDM	Internal	3.2(81)	6%T	15,647	100%T
CNG Cyl* Co. hoop-wrap	30° cutter	External	2.0(51)	5%t	8,036	100%t
PST-Steel* hoop wrap	30° cutter	External	2.0(51)	5%t	19,469	100%t

* the defect was cut through the entire composite and into the liner.



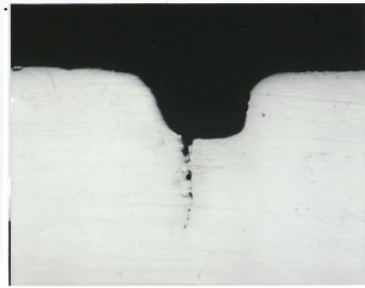
FABER Grinding Disc Flaw 24X

(a)



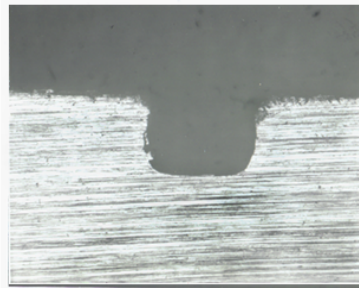
FABER 45 Flaw 50X

(b)



FABER 30 Flaw Plus
Fatigue Crack 50X

(c)



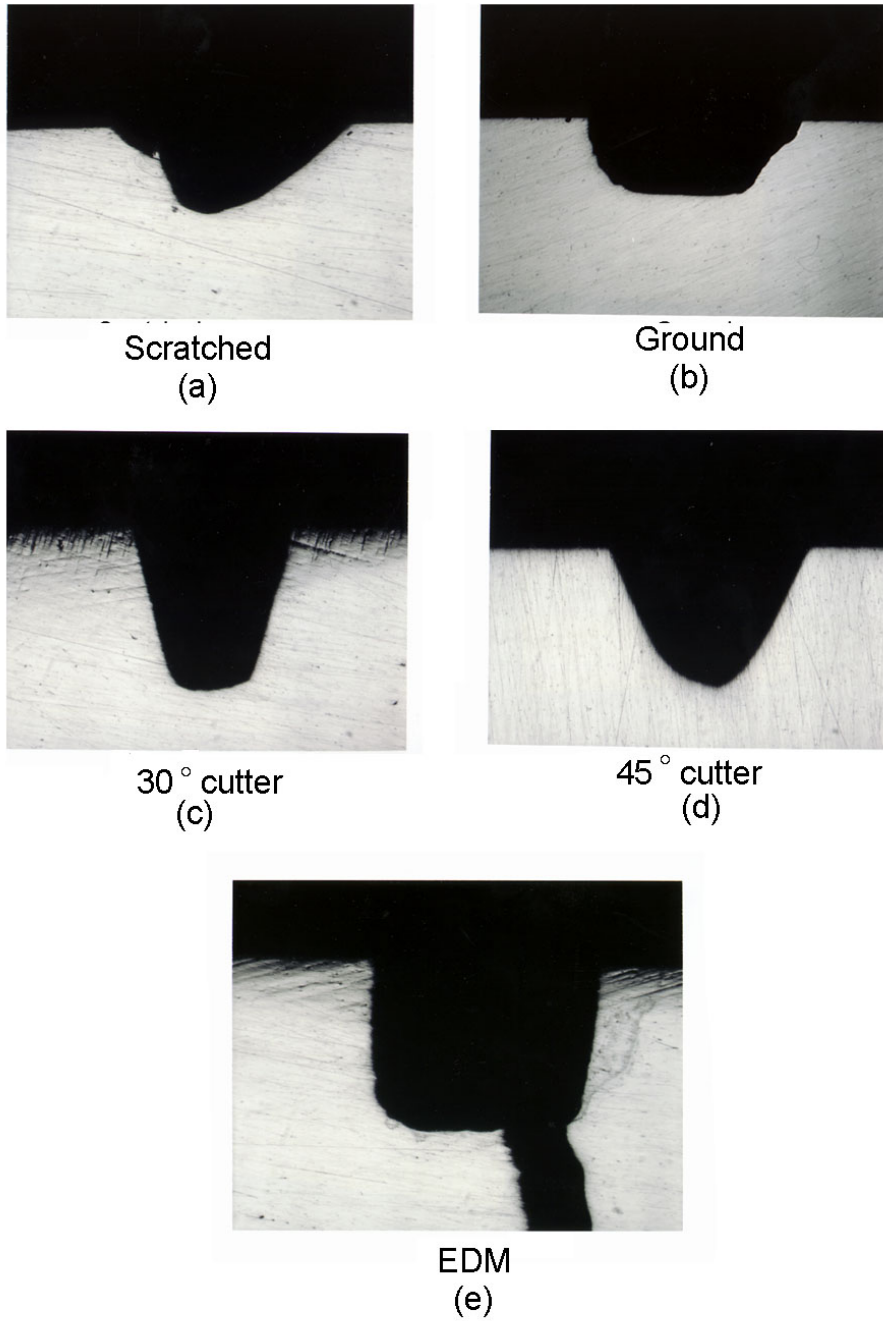
FABER EDM Flaw 50X

(d)



(e)

Figure A-23. Shape of the different 3 to 6% deep external defect introduced on an all-steel cylinder by various machining techniques: (a) by grinding; (b) using a 45° cutter; (c) using a 30° cutter; (d) by EDM method; (e) fracture surface of the leak.



gsb88g1

Figure A-24. Shape of the different 3 to 6% deep external defect introduced on an all-aluminum cylinder by various machining techniques: (a) using scriber; (b) by grinding; (c) using 30° cutter; (d) using 45° cutter; (e) EDM method.

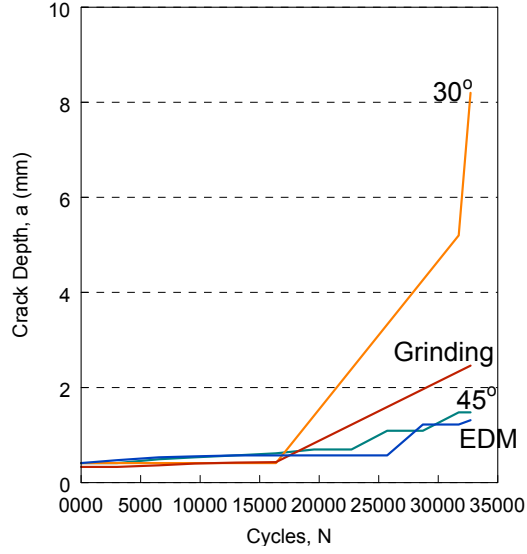


Figure A-25. Growth of fatigue crack from various 2 inch (51 mm) long 3 to 6% deep external defects introduced onto a Faber steel cylinder.

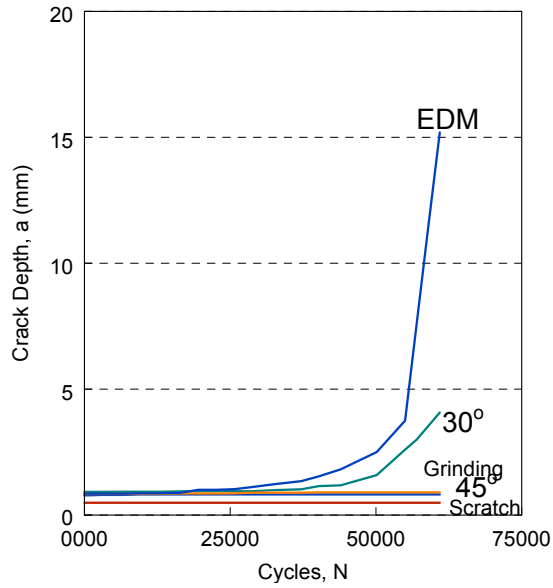


Figure A-26. Growth of fatigue crack from various 2 inch (51 mm) long external defects introduced onto a Luxfer all-aluminum (AA6061-T6) cylinder.

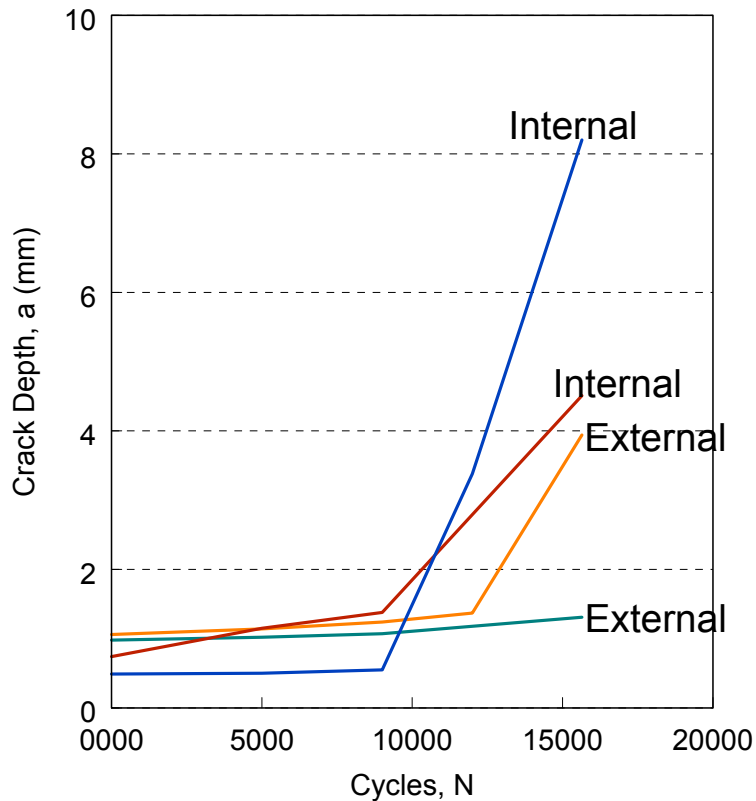


Figure A-27. Growth of fatigue cracks from EDM defects, introduced onto external and internal surfaces of a Faber all-steel cylinder.

On an aluminum hoop-wrapped and a steel hoop-wrapped cylinder, two inch (51 mm) long defects were machined onto the external surfaces. using a 30° CVN cutter. Defects were cut through the entire composite wrap, extending into the liner to 5% of its thickness. A fatigue crack which initiated from the machined defect caused a leak of the steel hoop-wrapped cylinder after 19,469 cycles, whereas the flawed aluminum hoop-wrapped cylinder leaked after 8,036 cycles.

APPENDIX B

**DEVELOPMENT OF PARAMETRIC EQUATION
FOR CRITICAL FLAW SIZE ESTIMATION FOR ALL-STEEL DESIGNS**

Prepared by:

M.P. Connolly, Ph.D.
Cyltek, Inc
310A Breesport
San Antonio, TX 78216

August 1997

Table of Contents

	<u>Page</u>
Executive Summary	
B1.0 Background to Flaw Size Calculations in the Cylinder Sidewall	B2
B1.1 Development of a Fracture Mechanics Model	B2
B1.2 Parametric Runs to Establish the Property Relationships	B4
B1.3 Statistical Analysis of the Data	B6
B1.4 Comparison of the Parametric Equations with Cylinder Test Data	B9
B1.5 Discussion	B10

B1.0 Background to Flaw Size Calculations in the Cylinder Sidewall.

The objective of this analysis was to develop an equation that could be used to predict the critical crack length for LBB without the need to perform a fracture mechanics analysis. For a particular cylinder, when the crack penetrates the sidewall the length of the crack determines whether a leak or rupture occurs. Therefore the crack length is used to define the flaw size and the two terms are used interchangeably.

The equation was developed for cracks in the cylinder sidewall. The equation cannot be used to account for cracks at the cylinder dome ends. However for all-metal cylinders the most likely location for cracks to occur is in the cylinder sidewall acted on by the hoop stress.

The equations that were developed were of the following form:

$$L_d = f(\text{Cylinder dimensions, Material properties, Operating conditions}) \quad (\text{B1})$$

where L_d is the calculated crack length for LBB. Cracks less than L_d should exhibit a leak when they penetrate the cylinder wall. Conversely cracks greater than L_d should exhibit a rupture. The key advantage of equation (B1) is that the user does not need to perform a detailed elastic-plastic analysis. The cylinder dimensions and material properties can be entered into the equations to predict the critical crack length for LBB.

The equations were developed as follows:

- (1) Perform a fracture mechanics analysis to predict the critical crack length for LBB.
- (2) Perform a large number of parametric runs to obtain the relationship between the critical crack length for LBB and the input conditions.
- (3) Use a statistical analysis package to obtain the functional relationships from the data in (3).
- (4) Compare the parametric equations with the results from the full-scale tests.

Each of the above four steps is now described in turn.

B1.1 Development of a Fracture Mechanics Model.

For most types of CNG cylinders the critical crack length is the crack length where the crack becomes unstable and causes the vessel to fail. This critical crack size is a function of the geometry of the cylinder, the geometry of the crack and the material properties. The concept of linear elastic fracture mechanics (LEFM) can be used to estimate the critical crack length. However this approach can be erroneous as a result of the influence of crack tip plasticity. Crack tip plasticity is the condition where a large plastic zone exists ahead of the crack tip - a situation not accounted for in LEFM.

For this situation elastic-plastic fracture mechanics (EPFM) techniques must be used. Commonly this involves use of the elastic crack tip parameter, termed J , which extends

the concepts of LEFM into the regime where crack-tip plasticity is important. For cases where the crack tip plasticity is negligible an elastic-plastic J integral type analysis will produce the same results as an LEFM analysis.

The approach that was adopted in the present analysis is based on the Failure Analysis Diagram (FAD) which has been widely applied for a number of years in the United States and Europe. Although the technique was originally developed for steel components in the nuclear power industry, the advanced EPFM is now being applied in the aerospace industries. More recently the technique has been adopted as part of the fitness for service in the petrochemical industry through the use of the PREFIS code¹. In Europe, the methodology forms the basis of the British Standards Institute document PD 6493².

Figure 1-1 shows a typical FAD diagram which consists of two axes. The vertical K_r axis provides an indication of the resistance of the structure to brittle fracture, the horizontal axis, L_r indicates the resistance of the remaining ligament ahead of the crack tip to plastic collapse. More formally the parameter K_r is defined as the ratio of applied stress intensity factor, K , to the fracture toughness of the material, K_{Ic} . The other parameter L_r is defined as the ratio of net sectional stress at the crack, S_n , to the yield stress of the material S_y .

In order to understand the overall approach consider an assessment point on the FAD curve (K_r^* , L_r^*) as shown in Figure 1-1. The interpretation of this assessment point is as follows. The value of K_r^* is a measure of the nearness of the structure to fast fracture. The value of L_r^* is a measure of the nearness of the structure to general yielding. The FAD diagram provides a means of interpolating between these two extremes.

The FAD curve is given in a form such as the following:

$$K_r = (1 - 0.14 L_r^2) [0.3 + 0.7 \exp. (-0.65 L_r^6)] \quad (B2)$$

If the assessment point falls inside the failure curve, then the structure is deemed to be safe. If the assessment point falls outside the curve then failure may occur. As the crack increases in size due, for example, to fatigue crack growth the associated assessment point for the crack moves closer to the FAD curve. When the crack is very large and the assessment point lies outside the curve then failure is deemed to occur.

This approach is likely to be very conservative as a result of the fact that the resistance to crack extension increases as the crack grows. This condition is more difficult to analyze, but can also be analyzed from a J instability analysis. Essentially, instability will occur when both of the following conditions are met:

$$J (\text{Driving Force}): J_D = J (\text{Resistance}): J_{mat} \quad (B3)$$

¹ Buchheim, G. M. et al., "Update of Fitness-for-Service and Inspection for the Petrochemical Industry" ASME PVP Vol. 288. 1994, pp. 253-260.

² British Standards Institute, 1991 "Guidance Methods for Assessing the Acceptability of Flaws in Fusion Welded Structures" PD 6493, 1991.

and

$$\frac{dJ_D}{da} > \frac{dJ_{mar}}{da} \quad (B4)$$

This instability analysis is shown schematically in Figure 1-2. The above analysis has been incorporated into a code termed C-LBB which was used to calculate the critical crack length for LBB in high pressure gas cylinders. This program requires the following inputs:

- (1) Cylinder dimensions: wall thickness, radius.
- (2) Internal pressure.
- (3) Tensile test properties: yield and tensile strength.
- (4) Resistance curve and fracture toughness.

The program models the crack as a through wall crack and equations have been obtained for the stress intensity factor and the limit load. For the stress intensity factor, equations based on Frenk's solution for the influence of transverse shear on an axial crack in a cylindrical shell were used.³

For the limit load the following equation was used, based on solutions from Kiefner⁴ and using the original Folias correction factor:

$$\sigma_n = \left(1.2 \left(1 + 3.2 \left(\frac{a^2}{DT} \right) \right)^{0.5} \right) \sigma_H \quad (B5)$$

Where a is the crack half length, D is the cylinder diameter, T is the cylinder wall thickness and σ_H is the hoop stress.

B1.2 Parametric Runs to Establish the Property Relationships.

The C-LBB program was exercised for a number of cases and it was determined that the relationship between the critical crack length for LBB, and the cylinder and material properties for a crack in the cylinder sidewall can be represented in the following form:

$$L_D = f(RT, \sigma_H, \sigma_y, J_I) \quad (B6)$$

where:

³ S. Frenk "Influence of transverse shear on an axial crack in a cylindrical shell" Int. Journ. Of Fracture, 14 (1978) 123-143.

⁴ J. F. Kiefner, W. A. Maxey, R. J. Eiber and A. R. Duffy "Failure stress levels of flaws in pressurized cylinders" ASTM STP 536, pp 461-481, 1973

L_d is the critical crack length for rupture to occur
 R is the cylinder radius
 T is the wall thickness
 σ_H is the hoop stress
 σ_y is the yield strength
 J_l is the slope of the resistance curve.

Although the influence of the intercept of the resistance curve J_0 (which is equivalent to the fracture toughness K_{Ic}), was shown not to have a major influence on the LBB crack length it is included in the parametric equation for completeness. Therefore the full form of the parametric equation that will be developed is as follows:

$$L_d = f(RT, \sigma_H, \sigma_y, J_0, J_l) \quad (B7)$$

This equation was developed for the following ranges of values:

Cylinder Size (RT)

Cylinder sizes are typically in the range of 7 to 15 inches in diameter with wall thicknesses in the range of 0.2 to 0.45 inches. The corresponding range of RT is 0.7 inches² to 3.4 inches². Therefore the following range of cylinder sizes were used:

$$0.5 < RT < 5 \quad (B8)$$

where the units of RT are inches².

Hoop Stress (σ_H)

The hoop stress is directly related to the yield strength of the material. In general the hoop stress is approximately 50% of the yield strength. Since the yield strength typically varies from 110 ksi to 200 ksi (for ultra high strength steels) the following hoop stress range was used:

$$50 < \sigma_H < 100 \quad (B9)$$

where the units of σ_H are ksi.

Yield Strength (σ_y)

The typical yield strength varies from approximately 90 ksi to 200 ksi. Therefore the following range was used:

$$90 < \sigma_y < 200 \quad (B10)$$

where the units of σ_y are ksi.

Fracture Toughness J_0

J_0 represents the intercept of the resistance curve and is equivalent to J_{Ic} . For pressure vessel steels, J_{Ic} typically varies from 200 in-lb/in² to 800 in-lb/in². Therefore the following range of J_0 was used:

$$0.2 < J_0 < 1.0 \quad (B11)$$

where the units of J_0 are in-lb/in² x 10³ (that is, the value of J_0 divided by 1000)

Resistance Curve Slope J_1

J_1 represents the slope of the resistance curve. For very brittle materials J_1 is close to zero whereas for very tough steels J_1 can be large. The following range covers most material values:

$$0 < J_1 < 60 \quad (B12)$$

where the units of J_1 are in-lb/in³ x 10³.

B1.3 Statistical Analysis of the Data.

The purpose of the statistical analysis was to determine the form of equation (B7). To do this the statistical analysis package Minitab was used. Minitab is capable of performing standard least-squares linear regression type analysis.

From an examination of the functional relationship between L_d and the input terms a regression analysis was performed with the following form of the regression equation:

$$L_d = C \cdot RT^{B1} \cdot \sigma_H^{B2} \cdot \sigma_y^{B3} \cdot J_0^{B4} \cdot J_1^{B5} \quad (B13)$$

This equation cannot be used directly by Minitab. By taking the logarithms of both sides a regression equation was obtained. For this regression a fit was obtained, with an R² value of 97.3. R² represents the goodness of fit where an R² value of 100% represents a

perfect fit. The values of the individual coefficients obtained from this analysis are given in Table B1.

Table B1. Results for regression using equation (B13)

Variable	Coefficient	T
ln(Rt)	0.470	200.05
ln(Hoop)	-1.637	-212.83
ln(Yield)	0.879	101.53
ln(J ₀)	0.072	23.92
ln(J ₁)	0.334	227.95
Constant	2.446	44.78

The T values in Table B1 represent the influence of the different variables on the result. A high absolute T value represents a strong dependency. Negative T values represent an inverse dependency; i.e. an increase in the variable produces a decrease in the result.

Although a good fit was obtained with equation (B13), an examination of the data indicated that there were some problem residuals. The residuals represent the difference between the exact values and the values from the fitted equations.

From an examination of the residuals it was apparent that some of the poor fits occurred with the high hoop stress and low J_1 values. To increase the fit of these values an extra term ($B_6 \cdot \sigma_H^{J_1}$) was added to equation (B13) as follows:

$$L_d = C \cdot RT^{B_1} \cdot \sigma_H^{B_2} \cdot \sigma_y^{B_3} \cdot J_0^{B_4} \cdot J_1^{B_5} \cdot B_6 \cdot \sigma_H^{J_1} \quad (B14)$$

By using this term the results were improved and an R^2 of 98.2% was obtained. The coefficients are given in Table B2.

Table B2. Results for regression using equation (B14)

Variable	Coefficient	T
lnRt	0.470	245.34
lnHoop	-1.620	-257.34
lnYield	0.877	124.02
lnJ ₀	0.065	26.24
lnJ ₁	0.432	175.38
J1lnHoop	-0.002	-45.47
Constant	2.446	50.41

The final run was performed by filling in some extra terms to increase the accuracy. The final form of the equation that was used in the regression analysis is as follows:

$$L_d = 0.00038 \cdot RT^{0.473} \cdot \sigma_y^{2.087} \cdot J_1^{0.446} \cdot \sigma_H^{0.013J_1} \cdot \exp[-0.024\sigma_H - 0.008\sigma_y + 0.1J_0 - 0.064J_1] \quad (B15)$$

The regression analysis yielded a fit of 98.8%. A plot of the residuals is shown in Figure 1-3. The figure shows that most of the data is very tightly bunched around the zero residual. The final form of the equation is as follows:

$$L_d = 0.00038 \cdot RT^{0.473} \cdot \sigma_y^{2.087} \cdot J_1^{0.446} \cdot \sigma_H^{0.013J_1} \cdot \exp[-0.024\sigma_H - 0.008\sigma_y + 0.1J_0 - 0.064J_1] \quad (B16)$$

The above equation provides a very accurate fit to the critical crack length. The equation can be used to estimate the critical crack length without the need to perform a detailed fracture mechanics analysis. Care should be exercised in using SI units in the equation since this is not possible for the exponential terms. Each of the units should be converted to English before being used and then converted back to SI. The units for the equation are given in Table B3.

Table B3. Units for parametric equation

Term	Description	Units
L_d	Crack Length	inches
R	Outer Radius	inches
T	Wall thickness	inches
σ_y	Yield Strength	ksi
σ_H	Hoop Stress	ksi
J_0	Resistance Curve Intercept	in-lb/in ² x 10 ³
J_1	Resistance Curve Slope	in-lb/in ³ x 10 ³

The units of J_0 and J_1 need explanation. If the value of J_0 is 200 in-lb/in² then 0.2 should be inserted in the equation. Similarly the value of J_1 should also be divided by 1000 before inserting it into the equation.

The range of applicability for the terms in the equation are given in Table B4.

Table B4. Range of applicability of the terms in the parametric equations.

Term	Description	Range
RT	Cylinder size	$0.5 < RT < 5$
σ_y	Yield Strength	$90 < \sigma_y < 200$
σ_H	Hoop Stress	$50 < \sigma_H < 100$
J_0	Resistance Curve Intercept	$0.2 < J_0 < 1.0$
J_1	Resistance Curve Slope	$0 < J_1 < 60$

The parametric equations are now compared to the results from the full-scale tests .

B1.4 Comparison of the Parametric Equations with Cylinder Test Data.

In order to determine the accuracy of the parametric equations the results were compared with those from the full-scale tests and also from the literature data. The data was also compared with the LEFM approach to determine the relative accuracy of the proposed approaches.

The parametric equations were compared with three sets of data:

- (1) Full-scale tests performed as part of this program.
- (2) Full-scale DOT 3AA cylinder data from the ISO WG14 database.
- (3) Full-scale DOT 3T cylinder data from the ISO WG14 database.

The results from these comparison are now described in turn.

B1.4.1 Comparison with Full Scale Data from this Program.

A total of seven tests were performed on full scale cylinders and these tests are summarized in Table B5. The data in Table B5 is categorized by data sets. Data set A is the Faber data, set B is the Taylor-Wharton data.

The results from Table B5 are plotted in Figure 1-4 for data set A and in Figure 1-5 for data set B. Also shown in the figures are the predictions for the parametric equations and also the approach used in LEFM approach. Open circles in the figures indicate a leak and closed circle indicate a rupture. Unfortunately for the Faber case (Figure 1-4) no data was available on a cylinder that fractured, therefore the relative accuracy of the two approaches is not known. For the Taylor-Wharton case the results show that the parametric equations are conservative, whereas the LEFM approach over-predicts the critical crack length.

B1.4.2 Comparison with data from ISO WG14 database

ISO TC58 SC3 working group WG14 performed full-scale LBB tests on cylinders. The data on two important strength levels 105 ksi - 125 ksi, corresponding to DOT 3AA, and termed material B, and the strength level 135 ksi - 159 ksi corresponding to DOT 3T and termed material C, were analyzed since there is comprehensive data on both of these steels.

The test cylinders were taken at random from the existing inventory of the participating cylinder companies. Most cylinders were tested with flaws which were machined with a CVN cutter. The cylinders were pressurized monotonically with water at room temperature until failure occurred.

The first set of results are from the lower strength steel cylinders and these are given in Table B6. For brevity all of the data in the table could not be plotted. Therefore the first set of data in the Table B6 corresponding to the 9.29 in diameter cylinders and termed data set C was plotted and the results are shown in Figure 1-6. As shown in Figure 1-6 the predictions from the parametric equations and the LEFM approach are similar. The reason for this improved prediction for the LEFM approach, as compared to the data in Figures 1-4 and 1-5, is due to the lower toughness of these cylinders, which is discussed in more detail below.

The results for the higher strength steel cylinders obtained from the WG14 database are given in Table B7. WG14 did not provide fracture toughness data therefore the fracture toughness values from the Faber cylinders were used since these cylinders had similar specifications.

For brevity only two of the data sets from Table B7 are plotted (F and G). Figure 1-7 shows the first set of data in Table B7 corresponding to the 9.02 inch diameter cylinders, and termed data set F and Figure 1-8 shows the results for data set G corresponding to the 8 inch diameter cylinders. Also shown in the figure are the predictions using the parametric equations and the LEFM. As shown in the figures the parametric equation predicts a larger flaw size than the data. However the predictions are substantially better than the LEFM approach which is very non-conservative for this case. This non-conservatism is due to the high ratio of toughness to strength for these materials an issue that is discussed below.

B1.5 Discussion

The parametric equations developed under this program can be used to predict the critical crack length for cracks in the cylinder sidewall. The results for the comparison with the data shows that the parametric equation predicts the experimental data reasonably well, and better than the current approach used in the LEFM approach. The reasons for these differences are now discussed.

The LEFM approach equivalent to only using the K_r part of the failure assessment diagram. This approach works well when this mechanism is the dominant failure mode. The competing failure mode is plastic collapse. The two material properties that govern these mechanisms are the fracture toughness (K_{Ic}), for fast fracture, and the yield strength (σ_y), for plastic collapse. The ratio of these properties defines the likely failure mechanism.

Case 1. Fracture Dominated: For the case where the fracture toughness (K_{Ic}), is relatively low compared to the yield strength (σ_y), then the failure will be fracture dominated. This is the case for the low toughness steels as in data set C (Figure 1-6). In this case the ratio of K_{Ic}/σ_y is approximately equal to 1. The results in Figure 1-6 show that the predictions for the parametric equations and the LEFM approach are very similar and are a close fit to the experimental data. This is unsurprising since the linear elastic fracture mechanics approach is based on the premise that failure will occur by fast fracture.

Case 2. Plastic Collapse Dominated: For the case where the fracture toughness (K_{Ic}), is high compared to the yield strength (σ_y), then the failure will be dominated by plastic collapse. This is the case for the high toughness steels such as the Faber steel cylinders (Figure 1-4) and also the WG14 data sets F and G (Figures 1-7 and 1-8). In this case the ratio of K_{Ic}/σ_y is greater than 1. The results in Figures 1-7 and 1-8 show that the predictions for the parametric equations and the LEFM approach are substantially different with the parametric equations predicting a lower critical crack length than the LEFM approach. This is due to the fact that the linear elastic fracture mechanics approach used in the standards does not take into account the plastic collapse failure mode. For example from Figure 1-7, for the case of a cylinder at service pressure the parametric equations predicts a critical crack length of 3.5 inches whereas the parametric equation predicts a crack length of approximately 5.2 inches.

The plastic collapse failure mode is important since most cylinders designed for NGV service will fall into Case 2 and therefore the current analysis requirements can be significantly non-conservative. The parametric equation provides a more accurate approach to analyzing the LBB requirements for cracks in the sidewall.

For cracks at the dome ends the equation cannot be used. However equations could also be developed for this case but would require an analysis similar to that performed here. Furthermore cracks in the dome are more likely to result in a rupture since the net section is thicker. Cracks at the dome are also more difficult to analyze since the dome section is much more sensitive to the details of the local design which may change slightly from cylinder to cylinder. One approach is to use the parametric equations for cracks in the sidewall. If the cylinder is likely to fail in the dome region then extensive testing should be required for cracks at that location.

Table B5.

Summary of results from the test performed under this program. The last four columns in the table provide the critical flaw length predictions for the parametric equation (Eqn.) and also the LEFM approach.

Data Set	No	Type	Test Type	D(in)	T(in)	a/T (%)	nT	l (in)	Ps (ksi)	Pf (psi)	Pf/Ps	Y (ksi)	U (ksi)	K1c	J0	J1	Failure	Eqn	LEFM	Eqn	LEFM
A	1	Faber	Hydraulic	12.44	0.32	80.00	10.2	3.284	3000	3750	1.25	125	139	194	1.14	56	Leak	3.40	4.32	Leak	Leak
A	2	Faber	Hydraulic	12.44	0.32	80.00	10	3.200	3000	3700	1.23	125	139	194	1.14	56	Leak	3.45	4.40	Leak	Leak
A	3	Faber	Hydraulic	12.44	0.32	80.00	12.4	3.968	3000	3220	1.07	125	139	194	1.14	56	Leak	3.95	5.10	Leak	Leak
B	6	Taylor-Wh.	Hydraulic	8.80	0.28	84.00	10	2.800	3000	3146	1.05	90	110	127	0.49	17.5	Leak	2.23	3.84	Frac	Leak
B	7	Taylor-Wh.	Pneumatic	8.80	0.28	90.00	10	2.800	3000	2830	0.95	90	110	127	0.49	17.5	Leak	2.45	4.36	Frac	Leak
B	8	Taylor-Wh.	Hydraulic	8.80	0.28	83.00	10	2.800	3000	3190	1.06	90	110	127	0.49	17.5	Leak	2.20	3.80	Frac	Leak
B	9	Taylor-Wh.	Pneumatic	8.80	0.28	80.00	10	2.800	3000	3200	1.07	90	110	127	0.49	17.5	Frac	2.19	3.76	Frac	Leak

Table B6.

Summary of results from the WG14 DOT3AA database (material B). The last four columns in the table provide the critical flaw length predictions for the parametric equation and also the LEFM approach. ($J_0 = 0.2, J_1 = 16$).

Data Set	No	Type	D(in)	T(in)	a/T (%)	nT	l (in)	Ps(ksi)	Pf (psi)	Pf/Ps	Y(ksi)	K1c	Failure	Eqn	LEFM	Eqn	LEFM
C	1	DOT3AA	9.29	0.30	67.00	3.4	1.00	3321	5497	1.66	84.06	81.10	Frac	0.97	0.84	Frac	Frac
C	2	DOT3AA	9.29	0.27	76.00	3.7	0.99	3220	5047	1.57	93.04	81.10	Frac	1.03	0.80	Leak	Frac
C	3	DOT3AA	9.29	0.29	86.00	3.4	0.98	3263	5221	1.60	87.97	81.10	LBB	1.05	0.86	Leak	Frac
C	4	DOT3AA	9.29	0.28	67.00	7	1.98	3017	4553	1.48	77.97	81.10	Frac	1.07	1.02	Frac	Frac
C	5	DOT3AA	9.29	0.28	76.00	7	1.98	3480	4902	1.41	100.00	81.10	Frac	1.29	0.90	Frac	Frac
C	6	DOT3AA	9.29	0.29	86.00	6.8	1.98	3278	4003	1.22	86.67	81.10	LBB	1.56	1.28	Frac	Frac
C	7	DOT3AA	9.29	0.27	67.00	9.9	2.69	3568	3916	1.10	106.96	81.10	Frac	1.86	1.18	Frac	Frac
C	8	DOT3AA	9.29	0.28	76.00	9.6	2.68	3292	3423	1.04	101.01	81.10	Frac	2.19	1.56	Frac	Frac
C	9	DOT3AA	9.29	0.28	86.00	9.5	2.69	3510	3553	1.01	100.87	81.10	LBB	2.09	1.44	Frac	Frac
C	10	DOT3AA	9.29	0.30	67.00	10	2.99	3611	4873	1.35	96.96	81.10	Frac	1.45	1.02	Frac	Frac
C	11	DOT3AA	9.29	0.28	76.00	10.6	3.00	3365	3887	1.16	95.94	81.10	Frac	1.75	1.28	Frac	Frac
C	12	DOT3AA	9.29	0.29	86.00	10.3	3.00	3452	2944	0.85	94.06	81.10	LBB	2.45	2.16	Frac	Frac
D	13	Spec	9.06	0.29	80.00	13	3.74	3771	3075	0.82	98.99	81.10	LBB	2.55	2.08	Frac	Frac
D	14	Spec	9.06	0.27	70.00	13	3.48	3510	4017	1.14	98.99	81.10	Frac	1.66	1.18	Frac	Frac
D	15	Spec	9.06	0.28	60.00	13	3.69	3713	446	1.21	98.99	81.10	Frac	1.51	1.04	Frac	Frac
D	16	Spec	9.06	0.29	75.00	13	3.74	3771	3655	0.97	98.99	81.10	LBB	2.01	1.44	Frac	Frac
D	17	Spec	9.06	0.27	71.00	13	3.53	3988	3379	0.85	128.99	81.10	Frac	2.83	1.56	Frac	Frac
D	18	Spec	9.06	0.30	72.00	13	3.89	4379	3771	0.86	128.99	81.10	Frac	2.97	1.56	Frac	Frac
D	19	Spec	9.06	0.30	75.00	13	3.89	4380	3147	0.72	128.99	81.10	LBB	3.58	2.10	Frac	Frac
D	20	Spec	9.06	0.29	78.00	13	3.74	4220	2901	0.69	128.99	81.10	LBB	3.68	2.26	Frac	Frac
D	21	Spec.	9.06	0.30	79.00	13	3.94	4438	3147	0.71	128.99	81.10	LBB	3.58	2.12	Frac	Frac
D	22	Spec.	9.06	0.31	83.00	13	3.99	4496	2553	0.57	128.99	81.10	LBB	4.42	3.20	Frac	Frac
D	23	DOT3AA	9.06	0.27	75.00	10	2.68	3234	3771	1.17	94.93	81.10	Frac	2.03	1.32	Frac	Frac

Data Set	No	Type	D(in)	T(in)	a/T (%)	nT	l (in)	Ps(ksi)	Pf (psi)	Pf/Ps	Y(ksi)	K1c	Failure	Eqn	LEFM	Eqn	LEFM
D	24	DOT3AA	9.06	0.26	80.00	10	2.60	3176	3495	1.10	95.22	81.10	LBB	1.78	1.38	Frac	Frac
D	25	DOT3AA	9.06	0.27	85.00	15	4.07	3670	2074	0.57	109.42	81.10	LBB	3.59	3.40	Frac	Frac
D	26	DOT3AA	9.06	0.25	80.00	10	2.48	2857	3193	1.12	83.62	81.10	LBB	1.55	1.50	Frac	Frac
D	27	DOT3AA	9.06	0.27	85.00	8	2.17	3147	3901	1.24	92.03	81.10	LBB	1.38	1.24	Frac	Frac
D	28	DOT3AA	9.06	0.26	70.00	15	3.96	2988	2814	0.94	95.36	81.10	Frac	2.26	2.00	Frac	Frac
C	29	DOT3AA	9.29	0.36	80.00	10	3.62	4264	4104	0.96	93.91	81.10	LBB	2.42	1.78	Frac	Frac
C	30	DOT3AA	9.29	0.38	75.00	10	3.82	4482	3901	0.87	93.91	81.10	Frac	2.76	2.10	Frac	Frac
C	31	DOT3AA	9.29	0.39	80.00	10	3.90	4568	3423	0.75	93.91	81.10	LBB	3.19	2.70	Frac	Frac
	32	DOT3AA	9.37	0.63	80.00	10	6.26	7280	6701	0.92	96.96	81.10	LBB	3.52	2.00	Frac	Frac
	33	DOT3AA	9.37	0.63	75.00	10	6.26	7280	6396	0.88	96.96	81.10	LBB	3.67	2.12	Frac	Frac
	34	DOT3AA	9.37	0.64	70.00	10	6.38	7411	7643	1.03	96.96	81.10	LBB	3.14	1.72	Frac	Frac
E	35	DOT3AA	7.01	0.21	50.70	7.6	1.62	3263	4757	1.46	82.61	81.10	Frac	0.79	0.88	Frac	Frac
E	36	DOT3AA	7.01	0.22	58.70	7.4	1.60	3336	4801	1.44	83.62	81.10	Frac	0.88	0.92	Frac	Frac
E	37	DOT3AA	7.01	0.22	70.90	7.6	1.68	3582	4699	1.31	84.64	81.10	Frac	0.92	0.94	Frac	Frac
E	38	DOT3AA	7.01	0.20	79.00	7.4	1.49	3132	4249	1.36	90.58	81.10	Frac	0.98	0.95	Frac	Frac
E	39	DOT3AA	7.01	0.20	91.10	7.6	1.56	3234	3597	1.11	90.29	81.10	LBB	1.24	1.24	Frac	Frac
E	40	DOT3AA	7.01	0.20	51.20	8.7	1.75	3060	4554	1.49	85.07	81.10	Frac	0.80	0.85	Frac	Frac
E	41	DOT3AA	7.01	0.21	59.70	8.4	1.79	3408	4496	1.32	81.59	81.10	Frac	0.86	0.94	Frac	Frac
E	42	DOT3AA	7.01	0.22	70.50	8.6	1.86	3466	4293	1.24	83.62	81.10	Frac	1.04	1.10	Frac	Frac
E	43	DOT3AA	7.01	0.21	79.50	8.5	1.77	3408	4104	1.20	92.03	81.10	Frac	1.16	1.10	Frac	Frac
E	44	DOT3AA	7.01	0.20	89.70	8.5	1.74	3380	3394	1.00	87.54	81.10	LBB	1.28	1.38	Frac	Frac
E	45	DOT3AA	7.01	0.22	50.40	10.1	2.19	3597	4656	1.29	78.41	81.10	Frac	0.84	0.96	Frac	Frac
E	46	DOT3AA	7.01	0.21	57.90	9.7	2.06	3147	4206	1.34	77.68	81.10	Frac	0.88	1.05	Frac	Frac
E	47	DOT3AA	7.01	0.21	70.90	10.2	2.13	3364	3843	1.14	84.35	81.10	Frac	1.13	1.22	Frac	Frac
E	48	DOT3AA	7.01	0.21	78.00	9.8	2.04	3408	3553	1.04	81.16	81.10	Frac	1.18	1.38	Frac	Frac
E	49	DOT3AA	7.01	0.21	90.90	10	2.09	3495	3104	0.89	91.30	81.10	LBB	1.62	1.76	Frac	Frac
E	50	DOT3AA	7.01	0.21	49.20	12.4	2.59	3364	3901	1.16	97.10	81.10	Frac	1.34	1.18	Frac	Frac
E	51	DOT3AA	7.01	0.20	62.60	13.1	2.58	3205	3553	1.11	86.81	81.10	Frac	1.19	1.27	Frac	Frac
E	52	DOT3AA	7.01	0.19	69.50	12.4	2.39	3104	3046	0.98	86.23	81.10	Frac	1.30	1.52	Frac	Frac

Data Set	No	Type	D(in)	T(in)	a/T (%)	nT	l (in)	Ps(ksi)	Pf (psi)	Pf/Ps	Y(ksi)	K1c	Failure	Eqn	LEFM	Eqn	LEFM
E	53	DOT3AA	7.01	0.21	77.90	12.2	2.59	3524	2901	0.82	93.19	81.10	Frac	1.78	1.98	Frac	Frac
E	54	DOT3AA	7.01	0.21	90.50	12.6	2.68	3539	2204	0.62	80.72	81.10	LBB	1.82	2.85	Frac	Frac
E	55	DOT3AA	7.01	0.21	80.10	15	3.19	3510	2306	0.66	89.13	81.10	LBB	2.02	2.72	Frac	Frac
E	56	DOT3AA	7.01	0.19	61.50	15.4	2.97	3248	3249	1.00	89.71	81.10	Frac	1.28	1.36	Frac	Frac
E	57	DOT3AA	7.01	0.20	68.10	14.6	2.93	3162	2756	0.87	87.39	81.10	Frac	1.60	1.94	Frac	Frac
E	58	DOT3AA	7.01	0.20	78.50	14.7	3.01	3452	2495	0.72	96.38	81.10	LBB	1.99	2.26	Frac	Frac
E	59	DOT3AA	7.01	0.22	88.90	14.9	3.23	3524	1494	0.42	90.29	81.10	LBB	2.71	4.60	Frac	Leak
D	60	DOT3AA	9.13	0.26	83.30	9.9	2.57	3495	2698	0.77	108.41	81.10	LBB	2.76	2.12	Frac	Frac
D	61	DOT3AA	9.13	0.24	83.70	10	2.44	3104	3191	1.03	103.33	81.10	LBB	1.92	1.38	Frac	Frac
D	62	DOT3AA	9.13	0.25	85.90	10.3	2.60	3379	3263	0.97	110.58	81.10	LBB	2.17	1.42	Frac	Frac

Table B7.

Summary of results from the WG14 DOT 3T database (material C). The last four columns in the table provide the critical flaw length predictions for the parametric equation and also the LEFM approach. ($J_0 = 1.14, J_I = 56$).

Data Set	No	Type	D(in)	T(in)	a/T (%)	nT	l (in)	Ps(ksi)	Pf (psi)	Pf/Ps	Y (ksi)	U (ksi)	K1c	Failure	Eqn	LEFM	Eqn	LEFM
F	1	Spec.	9.02	0.27	70.00	10	2.68	4148	5323	1.28	127	144	193.8	Frac	2.16	3.10	Frac	Leak
F	2	Spec.	9.02	0.27	70.00	10	2.68	4090	5323	1.30	127	144	193.8	Frac	2.16	3.10	Frac	Leak
F	3	Spec.	9.02	0.26	70.00	10	2.64	4090	5337	1.30	127	144	193.8	Frac	2.00	2.90	Frac	Leak
F	4	Spec.	9.02	0.27	75.00	10	2.68	4148	5047	1.22	127	144	193.8	LBB	2.32	3.30	Frac	Leak
F	5	Spec.	9.02	0.26	75.00	10	2.64	4090	4786	1.17	127	144	193.8	LBB	2.33	3.36	Frac	Leak
F	6	Spec.	9.02	0.27	72.00	10	2.68	4148	5149	1.24	127	144	193.8	Frac	2.26	3.22	Frac	Leak
F	7	Spec.	9.02	0.27	65.00	10	2.68	4148	5511	1.33	127	144	193.8	Frac	2.05	2.96	Frac	Leak
F	8	Spec.	9.02	0.27	70.00	10	2.68	4148	5366	1.29	127	144	193.8	Frac	2.14	3.06	Frac	Leak
F	9	Spec.	9.02	0.27	75.00	10	2.68	4119	4931	1.20	127	144	193.8	LBB	2.39	3.44	Frac	Leak
F	10	Spec.	9.02	0.26	75.00	10	2.64	4032	4931	1.22	127	144	193.8	LBB	2.35	3.22	Frac	Leak
F	11	Spec.	9.02	0.27	80.00	10	2.72	4061	4641	1.14	124	139	193.8	LBB	2.50	3.70	Frac	Leak
F	12	Spec.	9.02	0.26	80.00	10	2.68	4032	4351	1.08	127	144	193.8	LBB	2.60	3.74	Frac	Leak
F	13	Spec.	9.02	0.26	78.00	10	2.56	3974	4641	1.17	127	144	193.8	LBB	2.42	3.48	Frac	Leak
G	14	Spec.	7.99	0.26	75.00	10	2.64	4453	5366	1.21	124	139	193.8	LBB	2.16	3.36	Frac	Leak
G	15	Spec.	7.99	0.26	75.00	10	2.64	4453	5366	1.21	124	139	193.8	LBB	2.16	3.36	Frac	Leak
G	16	Spec.	7.99	0.26	75.00	10	2.60	4394	5004	1.14	124	139	193.8	LBB	2.34	3.64	Frac	Leak
G	17	Spec.	7.99	0.26	80.00	10	2.64	4453	5076	1.14	124	139	193.8	LBB	2.34	3.64	Frac	Leak
G	18	Spec.	7.99	0.26	80.00	10	2.56	4322	4931	1.14	124	139	193.8	LBB	2.38	3.72	Frac	Leak
G	19	Spec.	7.99	0.26	78.00	10	2.56	4322	5076	1.17	124	139	193.8	LBB	2.31	3.60	Frac	Leak
G	20	Spec.	7.99	0.26	70.00	10	2.60	4394	5540	1.26	124	139	193.8	Frac	2.07	3.24	Frac	Leak
G																		
G	21	Spec.	7.99	0.26	65.00	10	2.64	4453	5801	1.30	124	139	193.8	Frac	1.95	3.04	Frac	Leak
G	22	Spec.	7.99	0.25	75.00	10	2.52	4264	4757	1.12	124	139	193.8	LBB	2.33	3.64	Frac	Leak
G	23	Spec.	7.99	0.26	75.00	10	2.56	4322	5178	1.20	124	139	193.8	LBB	2.25	3.52	Frac	Leak
G	24	Spec.	7.99	0.25	70.00	10	2.52	4264	5584	1.31	124	139	193.8	Frac	1.91	3.00	Frac	Leak

Data Set	No	Type	D(in)	T(in)	a/T (%)	nT	l (in)	Ps(ksi)	Pf (psi)	Pf/Ps	Y (ksi)	U (ksi)	K1c	Failure	Eqn	LEFM	Eqn	LEFM
G	25	Spec.	7.99	0.24	70.00	10	2.44	4133	5613	1.36	124	139	193.8	Frac	1.75	2.80	Frac	Leak
G	26	Spec.	7.99	0.25	72.00	10	2.52	4264	5584	1.31	124	139	193.8	Frac	1.91	3.00	Frac	Leak
F	27	Spec.	9.06	0.30	73.00	13	3.84	4569	2901	0.63	130	144	193.8	Frac	4.11	6.90	Leak	Leak
F	28	Spec.	9.06	0.30	73.00	13	3.84	4569	2901	0.63	130	144	193.8	Frac	4.11	6.90	Leak	Leak
F	29	Spec.	9.06	0.27	77.00	13	3.53	4206	2466	0.59	130	144	193.8	LBB	3.98	7.00	Leak	Leak
F	30	Spec.	9.06	0.28	80.00	10	2.80	4322	3626	0.84	130	144	193.8	LBB	3.44	5.00	Leak	Leak
F	31	Spec.	9.06	0.26	78.50	10	2.56	3974	3916	0.99	130	144	193.8	LBB	2.95	4.20	Leak	Leak
F	32	Spec.	9.06	0.29	77.00	13	3.79	4278	2683	0.63	124	139	193.8	LBB	3.90	7.00	Leak	Leak
F	33	Spec.	9.06	0.29	77.00	13	3.79	4278	2683	0.63	124	139	193.8	LBB	3.90	7.10	Leak	Leak
F	34	Spec.	9.06	0.30	71.00	13	3.84	4336	3046	0.70	124	139	193.8	Frac	3.84	6.60	Frac	Leak
F	35	Spec.	9.06	0.29	78.00	10	2.87	4453	3843	0.86	133	144	193.8	Frac	3.53	5.00	Leak	Leak
F	36	Spec.	9.06	0.27	80.00	10	2.72	4206	3263	0.78	133	144	193.8	Frac	3.63	5.30	Leak	Leak
F	37	Spec.	9.06	0.26	76.00	10	2.60	3901	3945	1.01	121	140	193.8	LBB	2.71	4.10	Leak	Leak
F	38	Spec.	9.06	0.26	76.00	10	2.60	3901	3945	1.01	121	140	193.8	LBB	2.71	4.10	Leak	Leak
F	39	Spec.	9.06	0.28	80.00	10	2.76	4119	4423	1.07	121	140	193.8	LBB	2.61	4.10	Frac	Leak
F	40	Spec.	9.06	0.27	75.00	10	2.68	4003	4815	1.20	121	140	193.8	Frac	2.33	3.50	Frac	Leak
F	41	Spec.	9.06	0.29	70.00	10	2.91	4351	4902	1.13	121	140	193.8	Frac	2.54	3.84	Frac	Leak
F	42	Spec.	9.06	0.29	70.00	10	2.91	4351	5163	1.19	121	140	193.8	Frac	2.39	3.60	Frac	Leak
F	43	Spec.	9.06	0.30	75.00	10	2.95	4409	4685	1.06	121	140	193.8	LBB	2.80	4.00	Frac	Leak
F	44	Spec.	9.06	0.30	75.00	10	2.95	4409	4830	1.10	121	140	193.8	LBB	2.72	4.10	Frac	Leak
G	45	Spec.	7.99	0.27	74.00	10	2.70	4496	4714	1.05	123	140	193.8	LBB	2.62	4.05	Frac	Leak
G	46	Spec.	7.99	0.27	69.00	10	2.72	4554	5294	1.16	123	140	193.8	Frac	2.32	3.60	Frac	Leak
G	47	Spec.	7.99	0.26	70.00	10	2.61	4307	5453	1.27	123	140	193.8	LBB	2.10	3.30	Frac	Leak
G	48	Spec.	7.99	0.26	75.00	10	2.60	4365	5221	1.20	123	140	193.8	LBB	2.21	3.48	Frac	Leak
G	49	Spec.	7.99	0.27	67.00	10	2.68	4496	5874	1.31	123	140	193.8	Frac	2.03	3.20	Frac	Leak
G	50	Spec.	7.99	0.27	67.00	10	2.68	4496	5540	1.23	123	140	193.8	Frac	2.19	3.40	Frac	Leak
H	51	Spec.	9.25	0.27	85.00	10	2.68	4061	3234	0.80	130	145	193.8	LBB	3.55	5.30	Leak	Leak
H	52	Spec.	9.25	0.25	85.00	10	2.52	3727	3307	0.89	125	140	193.8	LBB	3.07	4.64	Leak	Leak
H	53	Spec.	9.25	0.26	80.00	10	2.64	3756	4133	1.10	120	136	193.8	LBB	2.54	3.88	Frac	Leak

Data Set	No	Type	D(in)	T(in)	a/T (%)	nT	l (in)	Ps(ksi)	Pf (psi)	Pf/Ps	Y (ksi)	U (ksi)	K1c	Failure Eqn	LEFM	Eqn	LEFM
H	54	Spec.	9.25	0.26	70.00	10	2.64	3945	4394	1.11	130	143	193.8	Frac	2.77 3.64	Leak	Leak
H	55	Spec.	9.25	0.24	85.00	10	2.36	3698	3307	0.89	136	149	193.8	LBB	3.19 4.36	Leak	Leak
H	56	Spec.	9.25	0.26	85.00	10	2.60	3408	3553	1.04	115	125	193.8	LBB	2.78 4.56	Leak	Leak
H	57	Spec.	9.25	0.25	75.00	10	2.48	3959	3901	0.99	142	155	193.8	LBB	3.03 3.92	Leak	Leak
H	58	Spec.	9.25	0.26	70.00	10	2.64	4177	4046	0.97	138	155	193.8	Frac	2.84 3.76	Leak	Leak
H	59	Spec.	9.25	0.27	75.00	10	2.68	4235	4090	0.97	138	155	193.8	Frac	3.14 4.12	Leak	Leak
H	60	Expt	9.37	0.31	75.00	8	2.46	4902	6004	1.22	145	155	193.8	Frac	2.61 3.12	Leak	Leak
H																	
H	61	expt	9.37	0.31	75.00	8	2.46	4902	6004	1.22	145	155	193.8	Frac	2.61 3.12	Leak	Leak
H	62	expt	9.37	0.29	85.00	8	2.31	4612	5004	1.08	145	155	193.8	LBB	2.94 3.60	Leak	Leak
H	63	expt	9.37	0.30	80.00	8	2.43	4859	5149	1.06	145	155	193.8	LBB	3.01 3.64	Leak	Leak
H	64	expt	9.37	0.26	80.00	6	1.56	4177	6294	1.51	145	155	193.8	Frac	1.64 2.12	Leak	Leak
H	65	expt	9.37	0.27	85.00	6	1.61	4307	6294	1.46	145	155	193.8	Frac	1.79 2.28	Leak	Leak
H	66	expt	9.37	0.27	90.00	6	1.61	4307	6004	1.39	145	155	193.8	LBB	1.95 2.44	Leak	Leak
H	67	iso 9809	7.52	0.26	85.00	10	2.56	4583	4830	1.05	122	139	193.8	LBB	2.47 4.04	Leak	Leak
H	68	iso 9809	7.52	0.26	85.00	10	2.56	4583	4830	1.05	122	139	193.8	LBB	2.47 4.04	Leak	Leak
H	69	iso 9809	7.52	0.25	88.00	10	2.48	4931	5120	1.04	140	139	193.8	LBB	2.53 3.56	Leak	Leak
F	70	iso 9809	9.13	0.19	86.00	9.9	1.83	3089	3698	1.20	145	155	193.8	LBB	2.10 2.80	Leak	Leak
F																	
F	71	spec.	9.13	0.19	86.00	10	1.87	2857	3292	1.15	133	143	193.8	LBB	2.24 3.20	Leak	Leak
F	72	spec.	9.13	0.19	83.00	10	1.93	2944	2843	0.97	133	143	193.8	LBB	2.61 3.64	Leak	Leak
F	73	spec.	9.13	0.19	85.00	10	1.85	2828	2770	0.98	133	143	193.8	LBB	2.67 3.76	Leak	Leak
F	74	spec.	9.13	0.19	85.00	10	1.85	2828	2770	0.98	133	143	193.8	LBB	2.67 3.76	Leak	Leak

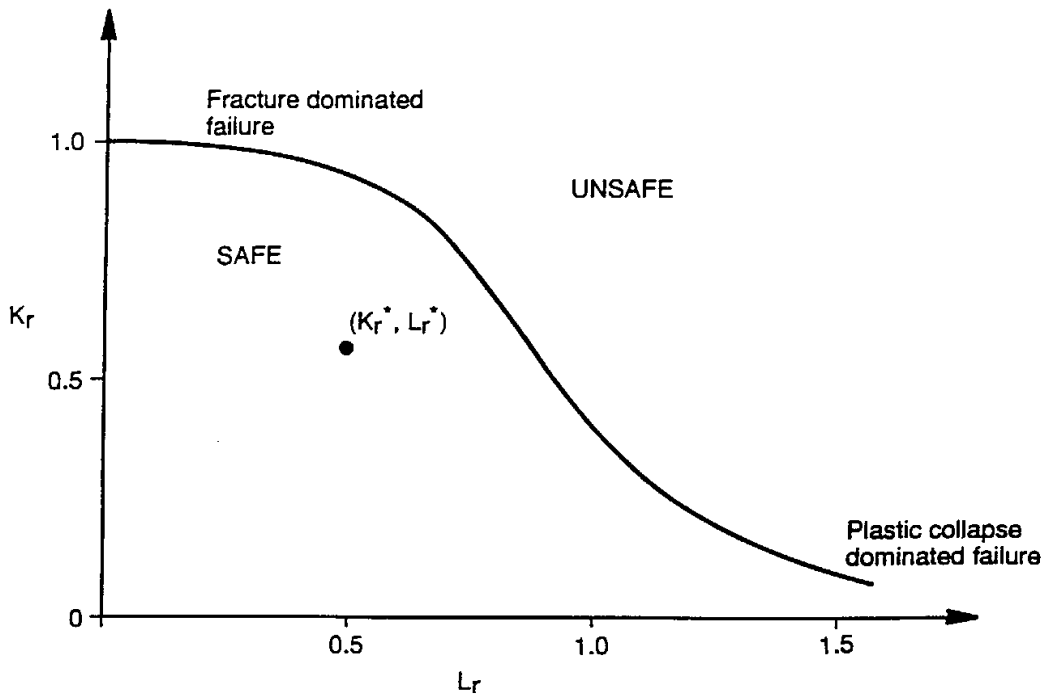


Figure 1-1. Failure Assessment Diagram (FAD) showing safe and unsafe regions.

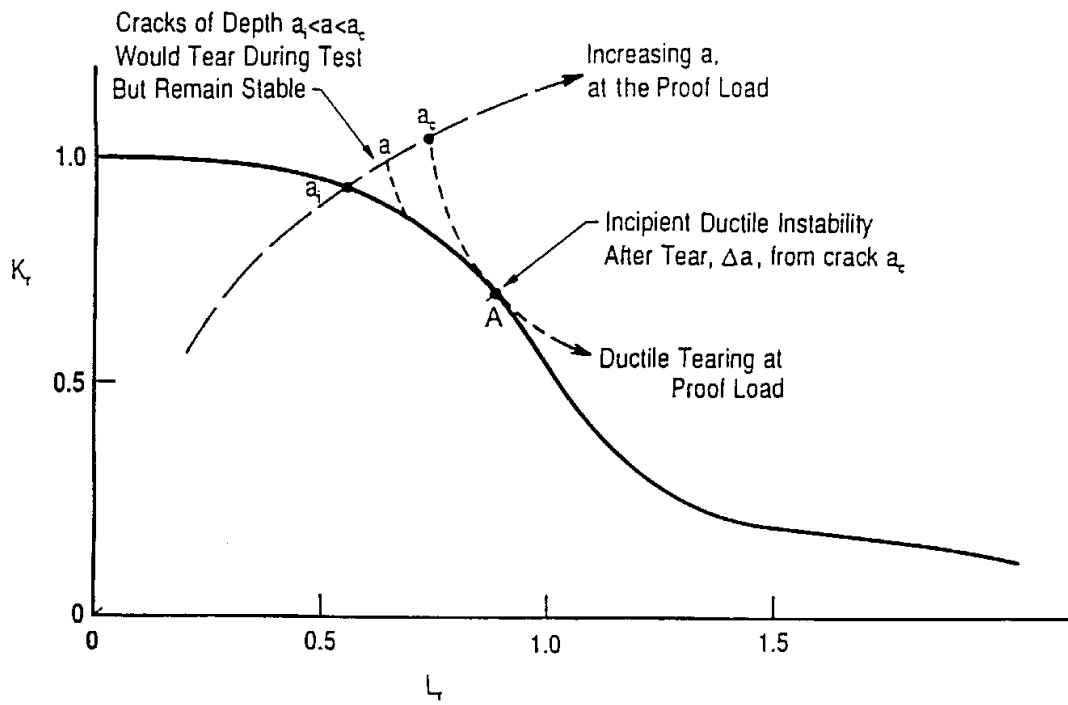


Figure 1-2. Schematic of failure assessment diagram showing calculation of critical crack size.

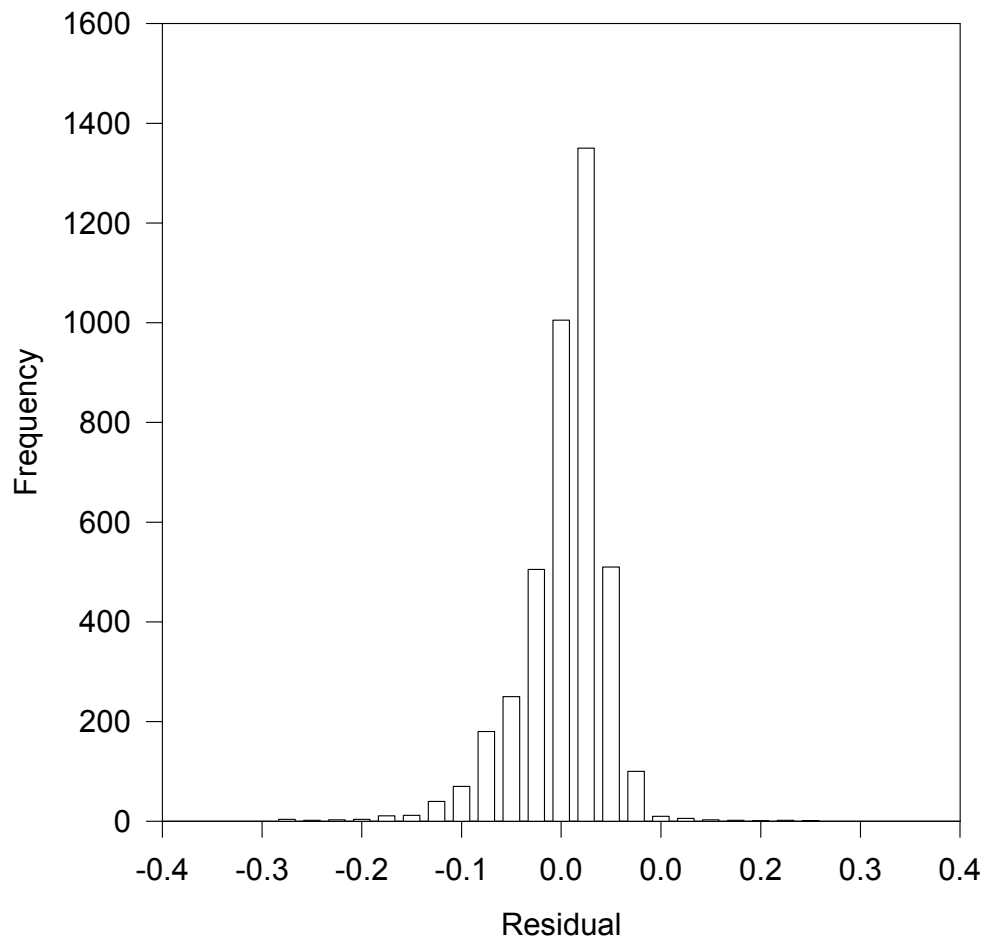
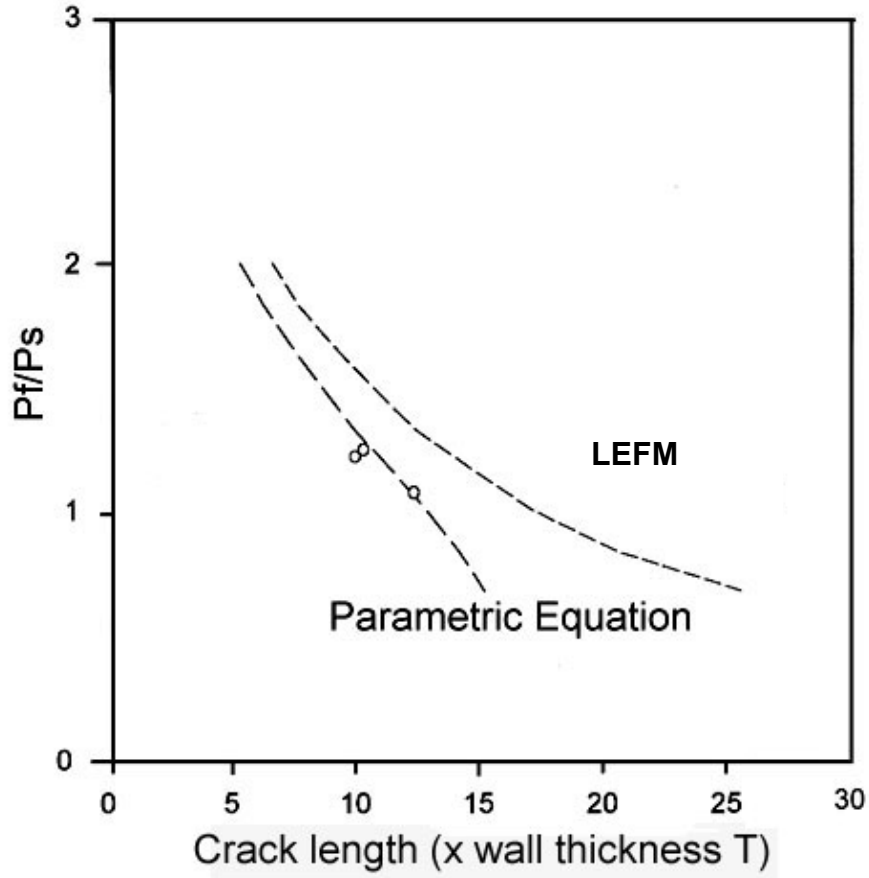
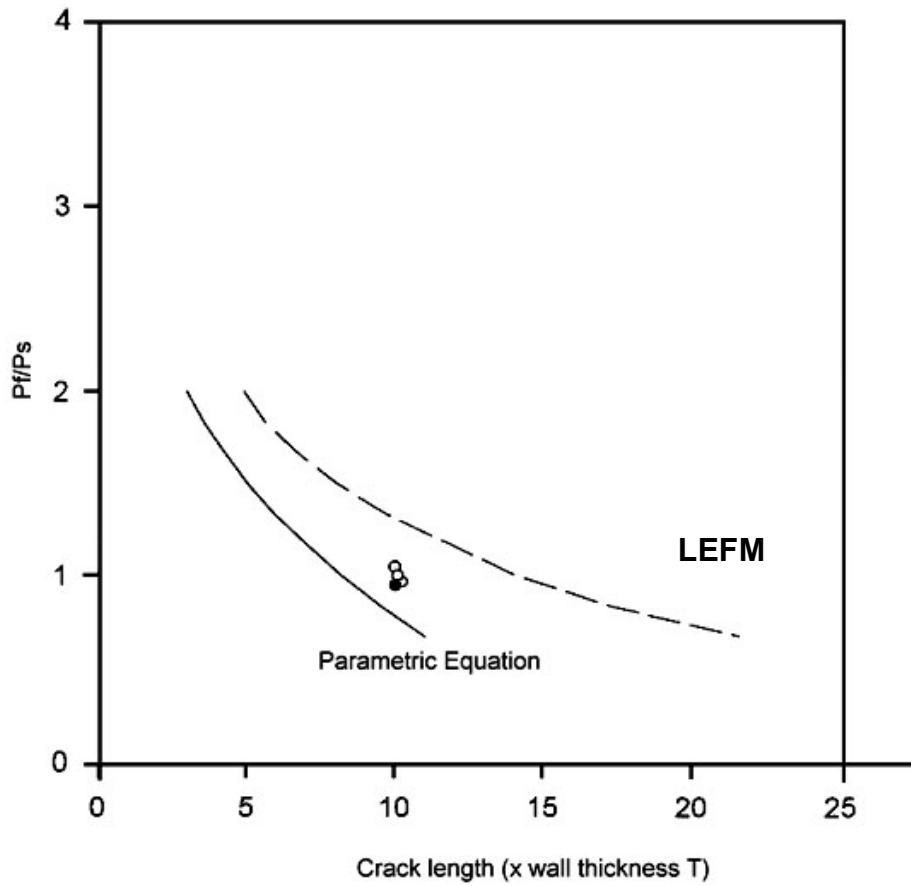


Figure 1-3 Histogram of the residual from final form of the parametric equation. The residual represent the difference between the exact and computed values.



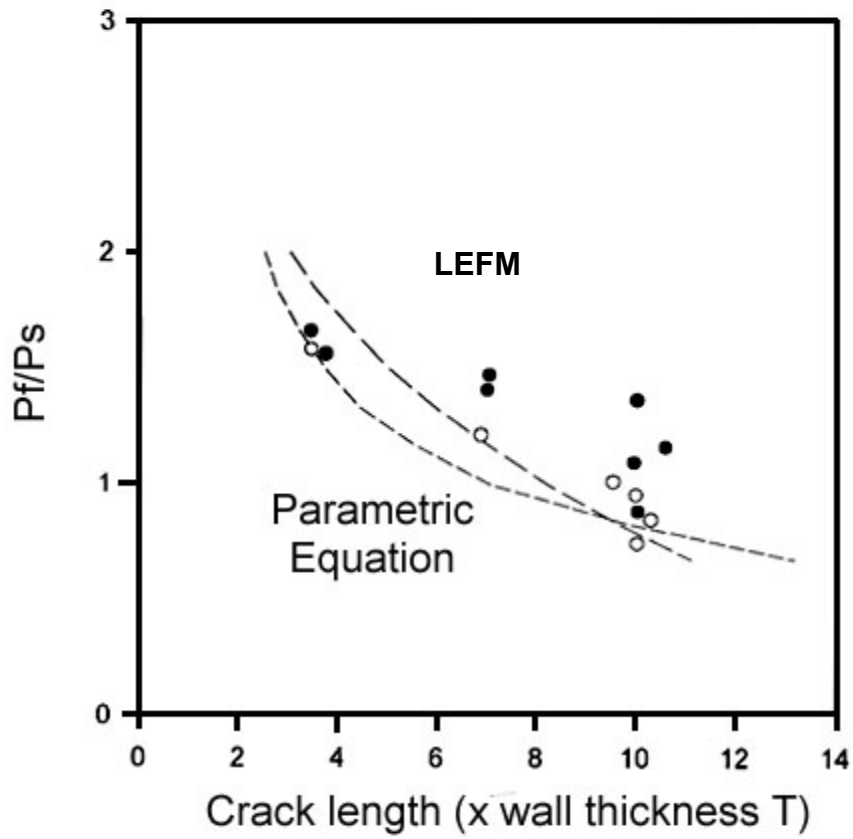
gsb138a

Figure 1-4 Comparison between parametric equations, the LEFM approach and the experimental data for the Data Set A. (Faber steel cylinder). Open circles indicate leak.



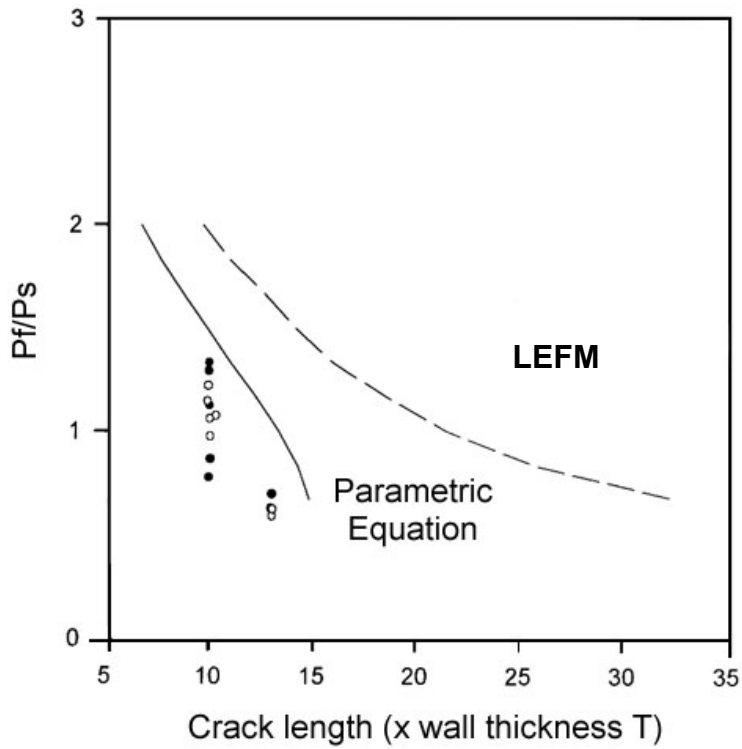
gib138b

Figure 1-5 Comparison between parametric equations, LEFM approach and the experimental data for the Data Set B. (Taylor-Wharton steel cylinder). Open circles indicate leak. Closed circles indicate fracture.



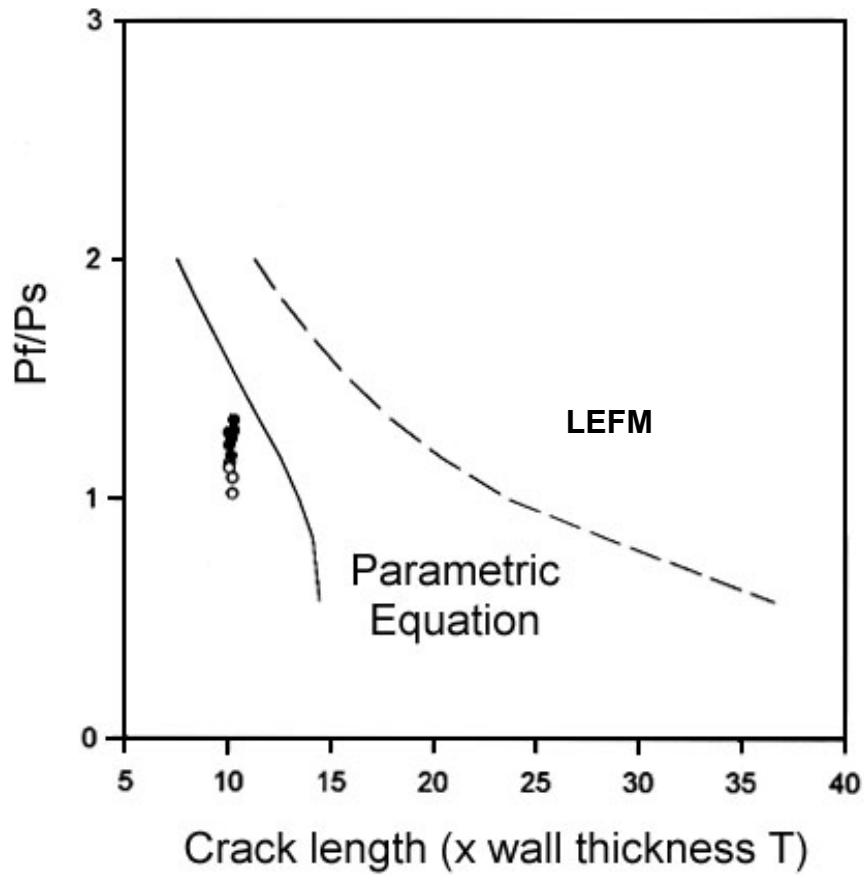
gsb138c

Figure 1-6 Comparison between parametric equations, LEFM approach and the experimental data for the Data Set C. (DOT 3AA WG14 steel cylinder). Open circles indicate leak. Closed circles indicate fracture.



gsb138d

Figure 1-7 Comparison between parametric equations, LEFM approach and the experimental data for the Data Set F. (DOT 3T WG14 steel cylinder). Open circles indicate leak. Closed circles indicate fracture.



gsb1383

Figure 1-8 Comparison between parametric equations, LEFM approach and the experimental data for the Data Set G. (DOT 3T WG14 steel cylinder). Open circles indicate leak. Closed circles indicate fracture.

APPENDIX C

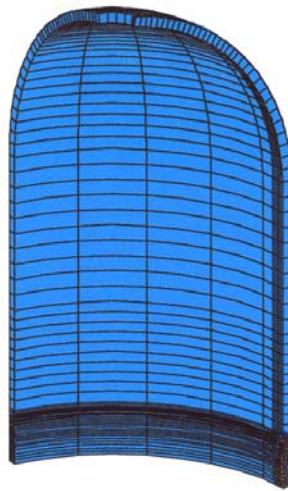
Numerical Fracture Analysis

Since one of the main goals of this project is to establish a simplified test method for assuring LBB performance of a design containing a deeper flaw (with a depth close to the wall thickness), it is important to establish whether an external deep axial flaw is more severe than an internal flaw of similar size. Elastic and elasto-plastic finite element analysis was carried out on the all-steel Faber design containing various deep internal and external axial cracks in order to compare crack driving forces for external axial semi-elliptical flaws with those for internal semi-elliptical flaws. Numerical fracture analysis of the all-steel cylinder design was carried out using the NISA finite element package****. Finite element models of the design containing axial cracks of various depths and lengths were modelled. Crack driving forces, such as stress intensity factor (K_I), crack opening displacement (COD) and J-integral values around the crack front were calculated for various crack depths and internal pressures.

The cylinder was modelled using solid elements. A finite element discretization of one eighth of the all-steel Faber design containing a 10T long internal axial flaw having a depth of 70% of the wall thickness is shown in Figure C-1. Von Mises stress distribution around the crack under an internal pressure of 3,750 psi (25.85 MPa) is shown in Figure C-2. Analyses were also carried out for a 10T long and 70% deep external flaw. Figure C-3 shows the crack driving force (stress intensity factor) at the deepest point of the semi-elliptical shaped external and internal cracks for an internal pressure of 3,750 psi (25.85 MPa). It can be seen that the crack driving force for the external crack is greater than that for the internal crack for crack depth greater than 20% of the wall thickness. A maximum crack driving force of $167 \text{ MPa}\sqrt{\text{m}}$, was obtained for a through-thickness ($a/T=1$) semi-elliptical shaped external crack. The maximum crack driving force for the external crack was approximately 14% higher than that for an internal crack.

Figure C-4 shows the effect of internal pressure on the J-integral for a 10T long and 70% deep internal axial crack. A J-integral value of 255 KJ/m^2 for the crack under an internal pressure of 3,750 psi (25.85 MPa) was obtained from the elasto-plastic finite element analysis, a value very close to the initiation fracture toughness ($J_{0.2}$) of the steel material of the Faber cylinder (see Table A-1).

**** NISA Finite Element Package, EMRC-NISA



83m-1

Figure C-1: Finite element model of the Faber steel cylinder with a 10T long axial internal flaw

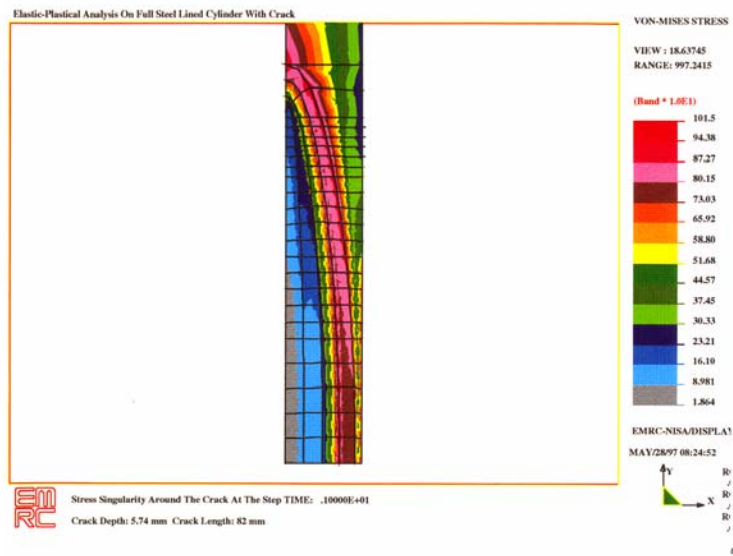
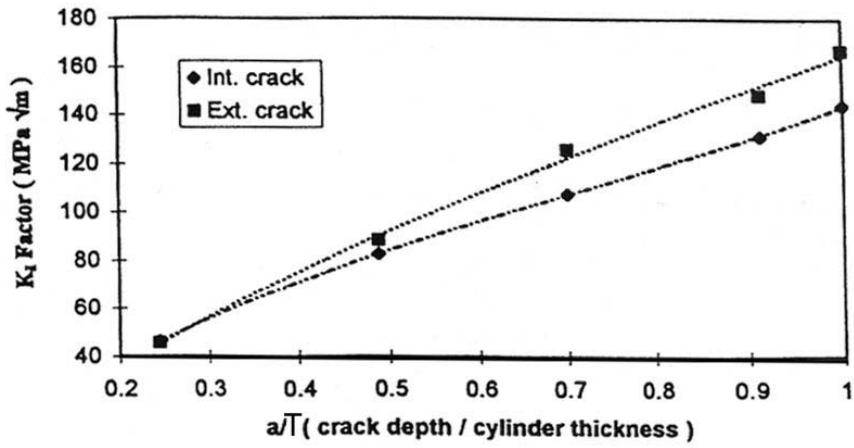
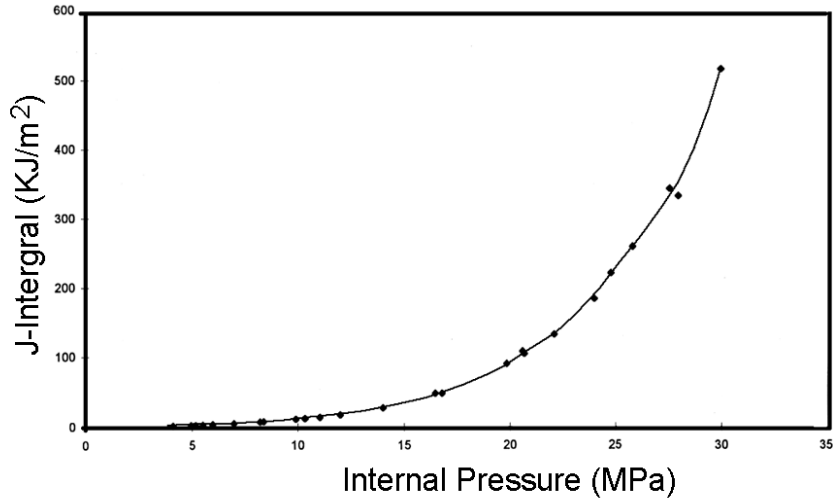


Figure C-2: Von-Mises stress contour of the Faber steel cylinder at an internal pressure of 3,750 psi [25.8 MPa] ahead of the crack front obtained from elasto-plastic analysis.



gsb88r

Figure C-3: Effect of crack depth of semi-elliptical internal & external surface crack on crack driving force in a Faber all-steel cylinder under a pressure of 3,750 psi (25.8 MPa)



88k

Figure C-4: J-integral values for a 10T long and 70% deep internal crack in Faber all-steel cylinder, under different pressures.